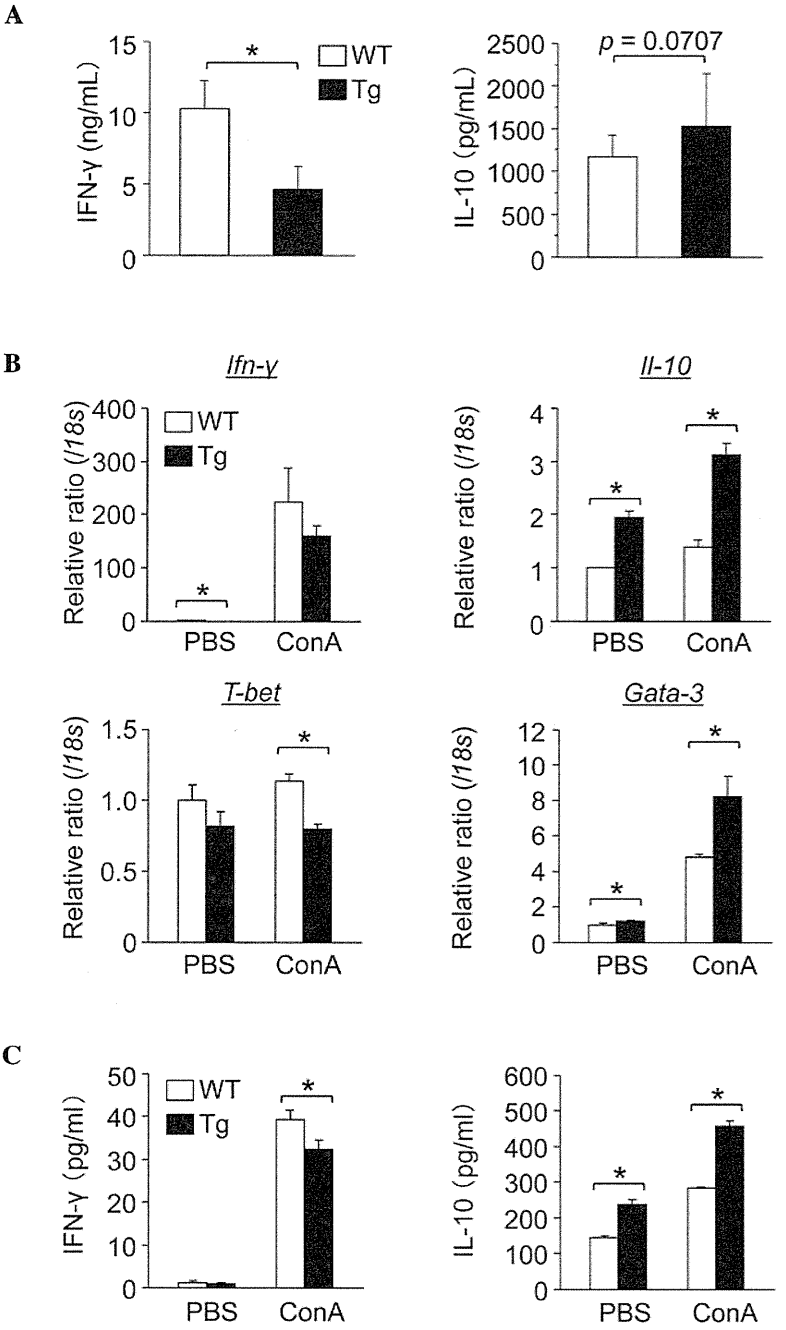

Figure 3. GnT-V Tg mouse splenic lymphocytes produce increased Th2 cytokines. (A) Anti-CD3/CD28 antibody-induced cytokine production levels secreted into the medium from splenic lymphocytes. Mononuclear cells of the spleen, isolated from WT and GnT-V Tg mice, were cultured for 48 h in the presence of anti-CD3 (5 μg/ml) and anti-CD28 (5 μg/ml) antibodies and levels of IFN-γ and IL-10 were measured using ELISA. The results are expressed as the mean ± standard deviation (n=3-8); *P<0.05. (B) Gene expression of cytokinines in the splenic lymphocytes following ConA stimulation is shown. Splenic lymphocytes from WT and GnT-V Tg mice were cultured for 24 h in the presence of ConA (5 μg/ml) and the gene expression levels of *Ifn-γ*, *Il-10*, *T-bet* and *Gata-3* were measured by reverse transcription quantitative polymerase chain reaction. The mRNA expression levels were normalized relative to that of *18s* and are expressed in arbitrary units. The results are expressed as the mean ± standard deviation (n=3); *P<0.05. (C) ConA-induced cytokine production levels secreted into the medium from splenic lymphocytes. Splenic lymphocytes from WT and GnT-V Tg mice were cultured for 24 h in the presence of ConA (5 μg/ml) and levels of IFN-γ and IL-10 were measured using ELISA. Results are expressed as the mean ± standard deviation (n=3); *P<0.05. WT, wild-type mouse splenic lymphocytes; GnT-V, *N*-acetylglucosaminyltransferase V; Tg, GnT-V transgenic mouse splenic lymphocytes; ConA, concanavalin A; BW, body weight; Ifn, interferon; IL, interleukin; PBS, phosphate-buffered saline; Th, T helper; CD, cluster of differentiation.

hepatitis in the GnT-V Tg mice *in vivo* was not explained by these *in vitro* results.

No difference is observed in the binding affinity of ConA to LSECs between WT and GnT-V Tg mice. The binding of ConA to the mannose gland of the LSEC surface, which is followed by LSEC damage, recruits T lymphocytes from the sinusoidal circulation and is an early event in T cell-mediated liver injury (5). The subsequent loss of function of the LSEC barrier exposes the underlying hepatocytes to further attack from activated T lymphocytes (5-7). To examine the binding affinity of ConA to LSECs from the WT and the GnT-V Tg mice, ConA lectin blotting and flow cytometric analysis were performed. The purity of the isolated LSECs was >75% (Fig. 4A).

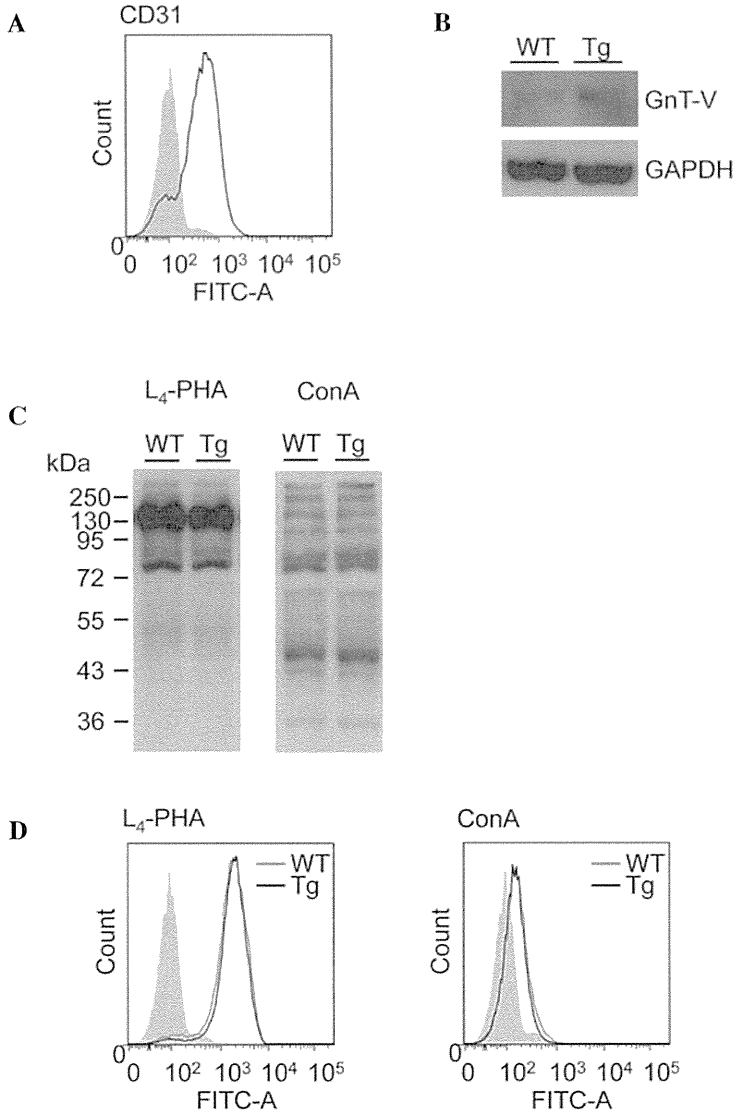

Figure 4. Binding affinity of ConA to LSECs does not differ between WT and GnT-V Tg mice. (A) Purity of the LSECs was analyzed by the expression of the cell surface marker, CD31. (B) Expression of GnT-V in LSECs was characterized by immunoblotting against GnT-V. Immunoblotting against GAPDH was performed as a loading control. (C) β1-6 *N*-acetylglucosamine branching (the product of GnT-V) and the binding affinity of ConA to LSECs were assessed by L_4-PHA and ConA by lectin blot analysis. (D) Results of the L_4-PHA and ConA lectin flow cytometric analysis. Data are representative of experiments repeated more than three times using three mice per experiment. WT, wild-type mouse LSECs; GnT-V, *N*-acetylglucosaminyltransferase V; Tg, GnT-V transgenic mouse LSECs; ConA, concanavalin A; LSEC, liver sinusoidal endothelial cell; CD, cluster of differentiation; L_4-PHA, leukoagglutinating phytohemagglutinin; FITC, fluorescein isothiocyanate.

To investigate the difference in the GnT-V and β1-6 GlcNAc branching of *N*-glycans expression in LSECs from the WT and GnT-V Tg mice, GnT-V immunoblotting, L_4-PHA lectin blotting and flow cytometric analysis were performed (Fig. 4B-D). L_4-PHA binds to the β1-6 GlcNAc branching of *N*-glycans, which is the product of GnT-V. Although the protein expression of GnT-V was increased in the GnT-V Tg mouse LSECs compared with the WT mouse LSECs (Fig. 4B), the expression of β1-6 GlcNAc branching of *N*-glycans, determined by L_4-PHA lectin blotting and flow cytometric analysis, did not differ between the WT and GnT-V Tg mouse LSECs (Fig. 4C, left panel and 4D, left panel). ConA lectin blotting and flow cytometric analysis also revealed no difference in the binding affinity of ConA to the LSECs between the WT and GnT-V Tg mouse LSECs (Fig. 4Cand D).

Number of hepatic macrophages is significantly increased in GnT-V Tg compared with WT mice. Subsequently, the hepatic immune cells were examined and the liver MNC subset was investigated prior to or following the injection of ConA. Notably, the number of CD11b-positive cells was significantly increased in the GnT-V Tg liver compared with the WT mouse liver prior to and 2 h after ConA injection (Fig. 5A and B). In addition, the gene expression of the macrophage markers F4/80 and CD68 were significantly increased in the Tg mouse MNCs (Fig. 5C). F4/80 immunohistochemical staining of the livers also revealed that the number of hepatic F4/80-positive macrophages was significantly increased in the GnT-V Tg mice compared with the WT mice (Fig. 6A and B). These results indicated that the number of hepatic macrophages was higher in the GnT-V Tg mice than in the WT mice.

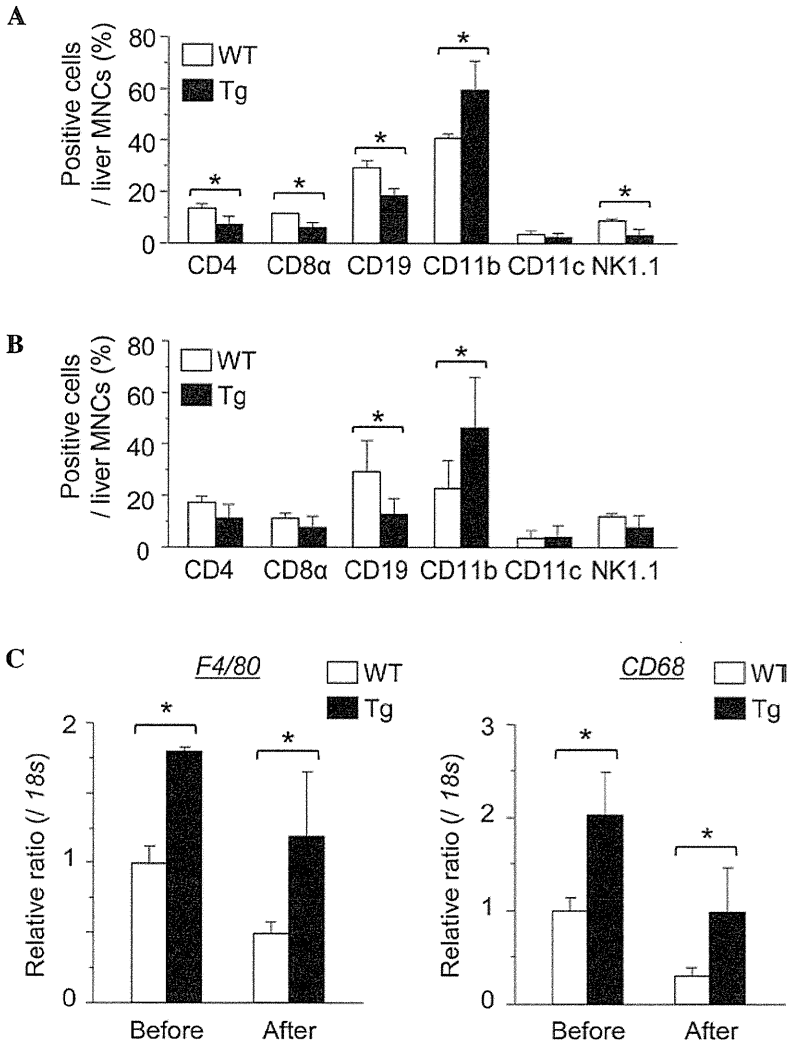

Figure 5. Hepatic macrophages are significantly increased in GnT-V Tg, vs. WT mice. Subset analyses of liver MNCs in the WT and GnT-V Tg mice (A) prior to and (B) 2 h after the injection of ConA at 12.5 mg/kg body weight were performed by flow cytometry. (C) Gene expression levels of the macrophage markers, F4/80 and CD68, in the MNCs before and 2 h after injection of ConA is shown. Results are expressed as the mean ± standard deviation (n=3); *P<0.05. WT, wild-type mouse liver MNCs; MNCs; ConA, concanavalin A; CD, cluster of differentiation; GnT-V, *N*-acetylglucosaminyltransferase V; Tg GnT-V, transgenic mouse liver; MNC, mononuclear cells.

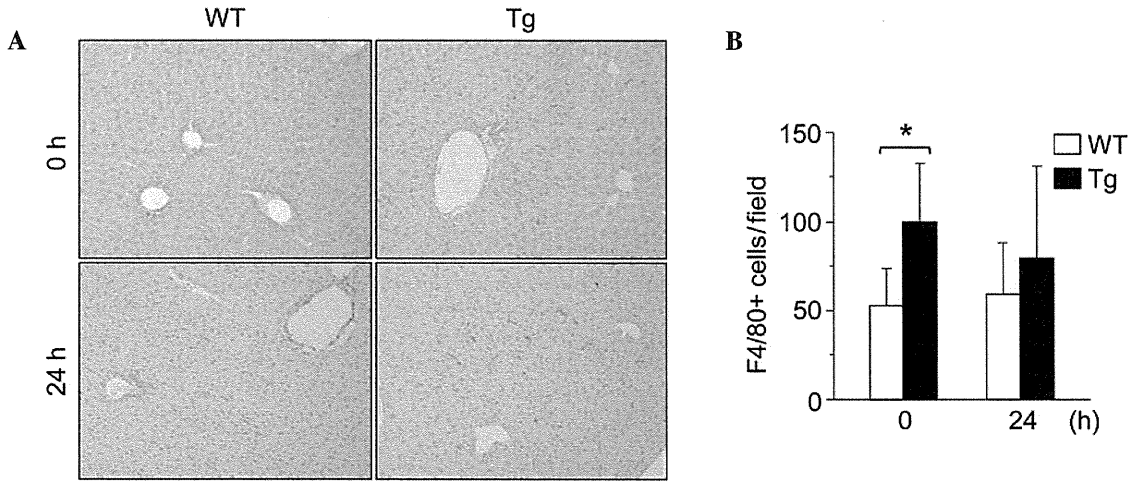

Figure 6. Number of hepatic F4/80-positive macrophages in GnT-V Tg mice is significantly increased compared with the number in WT mice. (A) Photomicrographs show representative mouse livers stained with anti-F4/80 antibody prior to (0 h) and 24 h after the injection of ConA at 12.5 mg/kg body weight (magnification, x200). (B) Quantification of the number of F4/80 positive cells/field is shown. Results are expressed as the mean ± standard deviation (0 h, n=9; 24 h, n=18); *P<0.05, compared with WT. WT, wild-type mouse liver; GnT-V, *N*-acetylglucosaminyltransferase V; Tg, GnT-V transgenic mouse liver; ConA, concanavalin A.

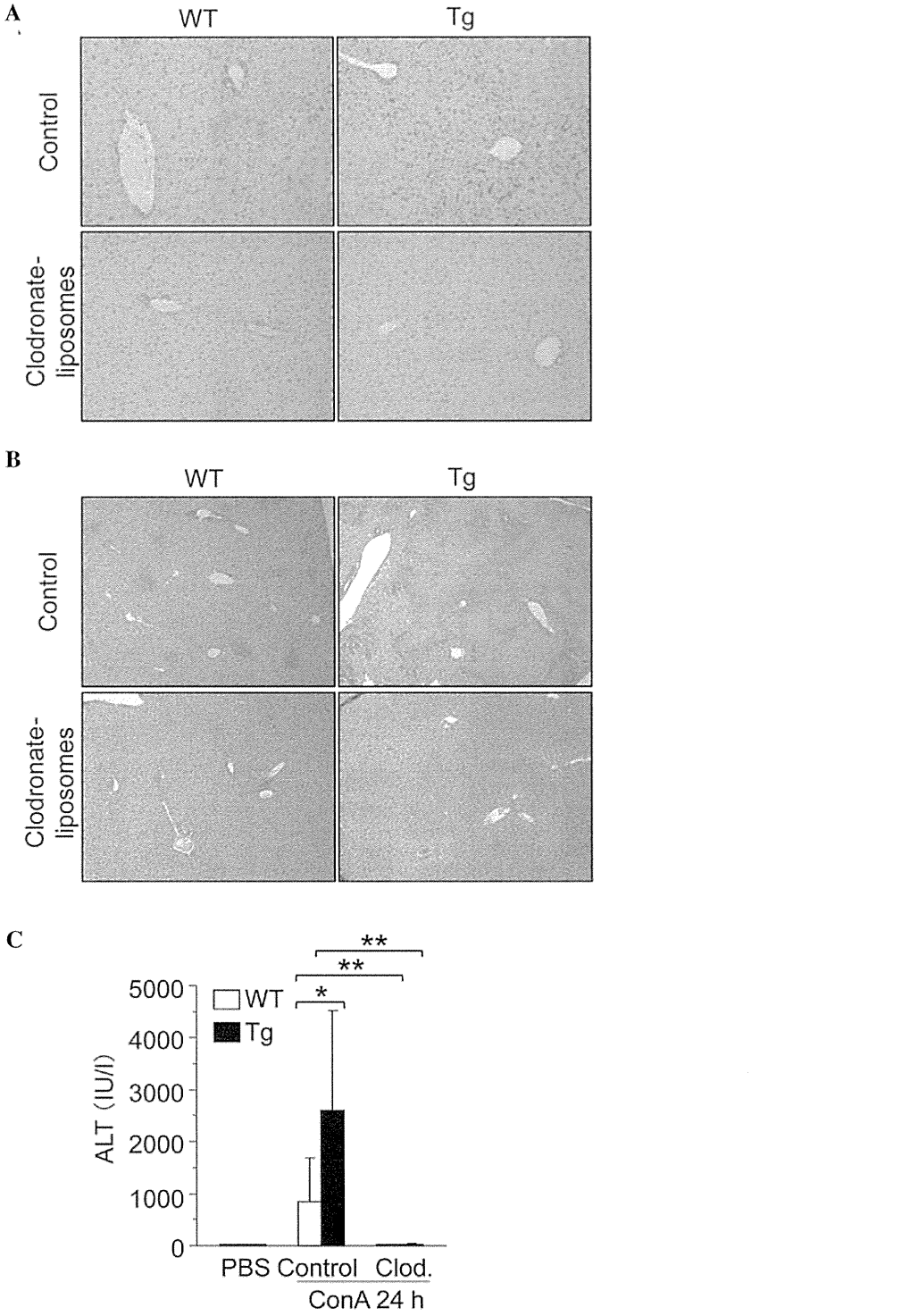

Figure 7. Hepatic macrophage depletion reduces the difference in the degree of hepatitis between WT and GnT-V Tg mice. (A) Representative photomicrographs mouse livers stained with anti-F4/80 antibody 24 h after the injection of ConA at 12.5 mg/kg BW (magnification, x200). Clodronate-liposomes were injected 2 days prior to ConA administration. (B) Representative photomicrographs of hematoxylin and eosin stained mouse livers 24 h after the injection of ConA at 12.5 mg/kg BW (magnification, x40). (C) Levels of serum ALT in mice (n=6) 24 h after the injection of ConA at 12.5 mg/kg BW. Results are expressed as the mean ± standard deviation; *P<0.05 and **P<0.01. WT, wild-type mice; GnT-V, *N*-acetylglucosaminyltransferase V; Tg, GnT-V transegenic mice; Clod, clodronate-liposomes; ALT, alanine aminotransferase; PBS, phosphate-buffered saline; ConA, concanavalin A; BW, body weight.

Depletion of hepatic macrophages reduces the degree of difference in ConA-induced hepatitis between WT and GnT-V Tg mice. To investigate the effect of hepatic macrophages in ConA-induced hepatitis in GnT-V Tg mice, macrophages were depleted from the WT and GnT-V Tg mice using clodronate-liposomes, and the severity of ConA-induced hepatitis was determined. The depletion of hepatic macrophages was confirmed by immunohistochemical staining with anti-F4/80 antibody (Fig. 7A). Macrophage depletion significantly suppressed ConA-induced liver injury in the WT and GnT-V Tg mice and it reduced the differences in liver injury between the WT and GnT-V Tg mice (Fig. 7B and C).

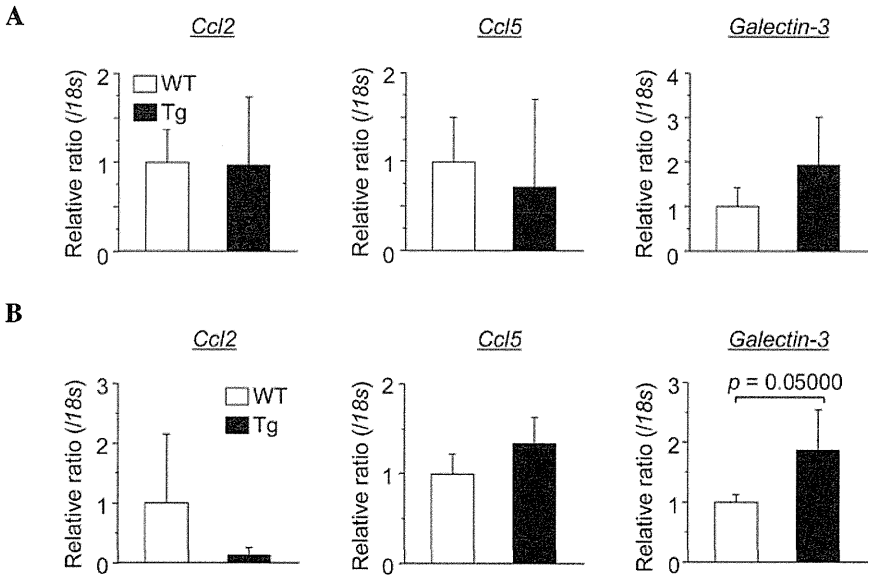

Figure 8. Gene expression of galectin-3 is elevated in Tg mouse hepatocytes. (A) Gene expression levels of macrophage chemoattractants in the mouse liver. (B) Gene expression levels of macrophage chemoattractants in the mouse hepatocytes. Results are expressed as the mean ± standard deviation. WT, wild-type mice; GnT-V, *N*-acetylglucosaminyltransferase V; Tg, GnT-V transgenic mice; Ccl, C-C chemokine ligand.

Expression of galectin-3 is elevated in Tg mouse hepatocytes. To elucidate the reason why the number of liver macrophages in the Tg mice was elevated compared with the number in the WT mice, the expression of macrophage chemoattractant genes (*Ccl2, Ccl5* and *Galectin-3*) were investigated in mouse hepatocytes (Fig. 8). The results demomnstrated that the gene expression of *galectin-3* was elevated in the Tg mouse hepatocytes compared with the WT mouse hepatocytes.

Discussion

In the present study, it was initially observed that ectopic expression of GnT-V exacerbated ConA-induced hepatitis despite the Th1 to Th2 cytokine shift observed in the GnT-V Tg mouse splenic lymphocytes. A relatively high dose of ConA induced a significantly higher mortality rate in the GnT-V Tg mice compared with the that in WT mice. The binding affinity of ConA to LSEC, which occurs in the first phase of ConA hepatitis, did not differ between the WT and GnT-V Tg mice. The results also revealed significant increases in hepatic macrophage infiltration in the GnT-V Tg mice liver compared with the WT mouse liver, prior to or following ConA injection. Notably, the gene expression of galectin-3, a hepatocyte and one of the major chemoattractants of macrophage, was increased in the Tg mice. These findings indicated that GnT-V-induced galectin-3 elevation recruited monocytes to the liver and resulted in an increased number of hepatic macrophages, ultimately leading to enhanced ConA-induced hepatitis in the Tg mice. The present study also observed that the depletion of macrophages inhibited and reduced the difference in the degree of ConA-induced hepatitis between the WT and GnT-V Tg mice. Considering these findings, the present study demonstrated that aberrant glycosylation, induced by GnT-V, increased hepatic macrophage infiltration and resulted in enhanced ConA-induced hepatitis.

In the liver, LSECs, Kupffer cells (hepatic macrophages), lymphocytes (T cells) and NK cells are involved in the immune response of ConA-induced hepatitis (5). Among these immune cells, T cells are critical in ConA-induced hepatitis (1,4,5). Therefore, to investigate the roles of GnT-V on T cell activation, splenic lymphocytes from WT and GnT-V Tg mice were stimulated with anti-CD3/CD28 antibodies or ConA *in vitro*. The GnT-V Tg mouse splenic lymphocytes produced lower levels of the IFN-γ Th1 cytokine and higher levels of the IL-10 Th2 cytokine compared with the WT mouse splenic lymphocytes. These findings were consistent with those of previous studies, which demonstrated that GnT-V-induced TCR oligosaccharide modification suppresses TCR signaling (22,23). However, these findings indicate that GnT-V tends to suppress inflammatory responses through suppression of T cell activation, which differ from the results of the present *in vivo* study.

ConA binds predominantly to LSECs within 15 min following intravenous injection. After 4 h, ConA begins to bind to hepatic macrophages (33), and activated lymphocytes are then trafficked towards hepatocytes, leading to inflammation (5,32). The present study hypothesized that the glycosylation differences between the LSECs of WT and GnT-V Tg mice may be important in the progression of ConA-induced hepatitis. To examine this hypothesis, differences in the lectin affinities of each mouse LSEC were investigated. It was found that ConA and L_4-PHA lectin bound equally to the WT and GnT-V Tg mouse LSECs, however, the expression of GnT-V was increased in the GnT-V Tg mice. Since levels of β1-6 GlcNAc branching are regulated by UDP-GlcNAc, a donor substrate of GnT-V (33), a change in the expression of GnT-V alone were insufficient to increase levels of β1-6 GlcNAc branching in the Tg mouse LSECs.

In response to these T cell and LSEC findings, the present study investigated hepatic macrophages as the main effector cell in the second phase of ConA-induced hepatitis (33,35). The hepatic macrophages were significantly increased in the

GnT-V Tg mice compared with the WT mice prior to and following ConA administration. It is understood that β1-6 GlcNAc branching extends repeated glycans of GlcNAc and galactose and results in a polylactosamine structure (36). Endogenous galectin-3 binds to this polylactosamine structure. Galectin-3 is a chemoattractant for monocytes and macrophages, which induces macrophage infiltration into the organs (35,37,38) and promotes inflammatory changes in various organs (35). Therefore, the polylactosamine structure induced in GnT-V Tg mice may increase the quantity of hepatic galectin-3. The present study also observed that the gene expression of galectin-3 was increased in the GnT-V Tg hepatocytes compared with the WT mouse hepatocytes. Therefore, GnT-V Tg mouse hepatocytes may produce higher quantities of galectin-3 than WT mouse hepatocytes. Increased hepatic galectin-3 in the GnT-V Tg mice may result in the elevated proportion of macrophages among the hepatic MNCs. In the present study, depletion of hepatic macrophages by clodronate-liposome infusion decreased the severity of ConA-induced hepatitis in the WT and GnT-V Tg mice and reduced the differences in liver injury between these mice. These results indicated that aberrant glycosylation by GnT-V elevated hepatic macrophage infiltration via an increase in hepatic galectin-3, exacerbating ConA-induced hepatitis. The reason for GnT-V-induced increases in hepatic galectin-3 and target glycoproteins for GnT-V in macrophages remains to be elucidated and its mechanisms require further investigation.

In conclusion, aberrant glycosylation by GnT-V led to increases in hepatic macrophage infiltration and enhanced ConA-induced hepatitis in mice. These findings indicate that the modulation of glycosylation may be a novel therapeutic target for immunity-associated acute hepatitis.

Acknowledgements

The present study was supported by Grants-in-Aid for Scientific Research (no. 21249038) and the Japan Society for the Promotion of Science (no. 24590972),.

References

1. Gantner F, Leist M, Lohse AW, Germann PG and Tiegs G: Concanavalin A-induced T-cell-mediated hepatic injury in mice: the role of tumor necrosis factor. Hepatology 21: 190-198, 1995.
2. Margalit M, Abu Gazala S, Alper R, *et al*: Glucocerebroside treatment ameliorates ConA hepatitis by inhibition of NKT lymphocytes. Am J Physiol Gastrointest Liver Physiol 289: G917-G925, 2005.
3. Takeda K, Hayakawa Y, Van Kaer L, Matsuda H, Yagita H and Okumura K: Critical contribution of liver natural killer T cells to a murine model of hepatitis. Proc Natl Acad Sci USA 97: 5498-5503, 2000.
4. Tiegs G, Hentschel J and Wendel A: A T cell-dependent experimental liver injury in mice inducible by concanavalin A J Clin Invest 90: 196-203, 1992.
5. Wang HX, Liu M, Weng SY, *et al*: Immune mechanisms of Concanavalin A model of autoimmune hepatitis. World J Gastroenterol 18: 119-125, 2012.
6. Yang MC, Chang CP and Lei HY: Endothelial cells are damaged by autophagic induction before hepatocytes in Con A-induced acute hepatitis. Int Immunol 22: 661-670, 2010.
7. Tsui TY, Obed A, Siu YT, *et al*: Carbon monoxide inhalation rescues mice from fulminant hepatitis through improving hepatic energy metabolism. Shock 27: 165-171, 2007.
8. Racanelli V and Rehermann B: The liver as an immunological organ. Hepatology 43: S54-S62, 2006.
9. Schrage A, Wechsung K, Neumann K, *et al*: Enhanced T cell transmigration across the murine liver sinusoidal endothelium is mediated by transcytosis and surface presentation of chemokines. Hepatology 48: 1262-1272, 2008.
10. Gove ME, Rhodes DH, Pini M, *et al*: Role of leptin receptor-induced STAT3 signaling in modulation of intestinal and hepatic inflammation in mice. J. Leukoc Biol 85: 491-496, 2009.
11. Takahashi K, Murakami M, Kikuchi H, Oshima Y and Kubohara Y: Derivatives of Dictyostelium differentiation-inducing factors promote mitogen-activated IL-2 production via AP-1 in Jurkat cells. Life Sci 88: 480-485, 2011.
12. Miller ML, Sun Y and Fu YX: Cutting edge: B and T lymphocyte attenuator signaling on NKT cells inhibits cytokine release and tissue injury in early immune responses. J Immunol 183: 32-36, 2009.
13. Boring L, Gosling J, Chensue SW, *et al*: Impaired monocyte migration and reduced type 1 (Th1) cytokine responses in C-C chemokine receptor 2 knockout mice. J Clin Invest 100: 2552-2561, 1997.
14. Kato M, Ikeda N, Matsushita E, Kaneko S and Kobayashi K: Involvement of IL-10, an anti-inflammatory cytokine in murine liver injury induced by Concanavalin A. Hepatol Res 20: 232-243, 2001.
15. Di Marco R, Xiang M, Zaccone P, *et al*: Concanavalin A-induced hepatitis in mice is prevented by interleukin (IL)-10 and exacerbated by endogenous IL-10 deficiency. Autoimmunity 31: 75-83, 1999.
16. Ohtsubo K and Marth JD: Glycosylation in cellular mechanisms of health and disease. Cell 126: 855-867, 2006.
17. Rademacher TW, Parekh RB and Dwek RA: Glycobiology. Annu Rev Biochem 57: 785-838, 1988.
18. Zhao Y, Sato Y, Isaji T, *et al*: Branched N-glycans regulate the biological functions of integrins and cadherins. FEBS J 275: 1939-1948, 2008.
19. Taniguchi N, Miyoshi E, Ko JH, Ikeda Y and Ihara Y: Implication of N-acetylglucosaminyltransferases III and V in cancer: gene regulation and signaling mechanism. Biochim Biophys Acta 1455: 287-300, 1999.
20. Lau KS and Dennis JW: N-Glycans in cancer progression. Glycobiology 18: 750-760, 2008.
21. Taniguchi N, Ihara S, Saito T, Miyoshi E, Ikeda Y and Honke K: Implication of GnT-V in cancer metastasis: a glycomic approach for identification of a target protein and its unique function as an angiogenic cofactor. Glycoconj J 18: 859-865, 2001.
22. Demetriou M, Granovsky M, Quaggin S and Dennis JW: Negative regulation of T-cell activation and autoimmunity by Mgat5 N-glycosylation. Nature 409: 733-739, 2001.
23. Li D, Li Y, Wu X, *et al*: Knockdown of Mgat5 inhibits breast cancer cell growth with activation of CD4+ T cells and macrophages. J. Immunol 180: 3158-3165, 2008.
24. Miyoshi E, Nishikawa A, Ihara Y, Gu J, *et al*: N-acetylglucosaminyltransferase III and V messenger RNA levels in LEC rats during hepatocarcinogenesis. Cancer Res 53: 3899-3902, 1993.
25. Miyoshi E, Ihara Y, Nishikawa A, *et al*: Gene expression of N-acetylglucosaminyltransferases III and V: a possible implication for liver regeneration. Hepatology 22: 1847-1855, 1995.
26. Kamada Y, Mori K, Matsumoto H, *et al*: N-Acetylglucosaminyltransferase V regulates TGF-beta response in hepatic stellate cells and the progression of steatohepatitis. Glycobiology 22: 778-787, 2012.
27. Terao M, Ishikawa A, Nakahara S, *et al*: Enhanced epithelial-mesenchymal transition-like phenotype in N-acetylglucosaminyltransferase V transgenic mouse skin promotes wound healing. J Biol Chem 286: 28303-28311, 2011.
28. Aicher WK, Fujihashi K, Yamamoto M, Kiyono H, Pitts AM and McGhee JR: Effects of the lpr/lpr mutation on T and B cell populations in the lamina propria of the small intestine, a mucosal effector site. Int Immunol 4: 959-968, 1992.
29. Kristensen DB, Kawada N, Imamura K, *et al*: Proteome analysis of rat hepatic stellate cells. Hepatology 32: 268-277, 2000.
30. Trobonjaca Z, Leithauser F, Moller P, Schirmbeck R and Reimann J: Activating immunity in the liver. I. Liver dendritic cells (but not hepatocytes) are potent activators of IFN-gamma release by liver NKT cells. J. Immunol 167: 1413-1422, 2001.
31. Shinzaki S, Iijima H, Fujii H, *et al*: Altered oligosaccharide structures reduce colitis induction in mice defective in beta-1,4-galactosyltransferase. Gastroenterology 142: 1172-1182, 2012.
32. Van Rooijen N and Sanders A: Liposome mediated depletion of macrophages: mechanism of action, preparation of liposomes and applications. J Immunol Methods 174: 83-93, 1994.

33. Knolle PA, Gerken G, Loser E, *et al*: Role of sinusoidal endothelial cells of the liver in concanavalin A-induced hepatic injury in mice. Hepatology 24: 824-829, 1996.
34. Sasai K, Ikeda Y, Fujii T, Tsuda T and Taniguchi N: UDP-GlcNAc concentration is an important factor in the biosynthesis of beta1,6-branched oligosaccharides: regulation based on the kinetic properties of N-acetylglucosaminyltransferase V. Glycobiology 12: 119-127, 2002.
35. Bacigalupo ML, Manzi M, Rabinovich GA and Troncoso MF: Hierarchical and selective roles of galectins in hepatocarcinogenesis, liver fibrosis and inflammation of hepatocellular carcinoma. World J Gastroenterol 19: 8831-8849, 2013.
36. Lee RT and Lee YC: Affinity enhancement by multivalent lectin-carbohydrate interaction. Glycoconj J 17: 543-551, 2000.
37. Sano H, Hsu DK, Yu L, *et al*: Human galectin-3 is a novel chemoattractant for monocytes and macrophages. J Immunol 165: 2156-2164, 2000.
38. Volarevic V, Milovanovic M, Ljujic B, *et al*: Galectin-3 deficiency prevents concanavalin A-induced hepatitis in mice. Hepatology 55: 1954-1964, 2012.

Journal of proteome research

Article

pubs.acs.org/jpr

Identification of Sialylated Glycoproteins in Doxorubicin-Treated Hepatoma Cells with Glycoproteomic Analyses

Kanako Azuma,[†] Satoshi Serada,[‡] Shinji Takamatsu,[†] Naoko Terao,[†] Shunsaku Takeishi,[§] Yoshihiro Kamada,[†] Tetsuji Naka,[‡] and Eiji Miyoshi*[,†]

[†]Department of Molecular Biochemistry & Clinical Investigation, Osaka University Graduate School of Medicine, Osaka 565-0871, Japan

[‡]Laboratory for Immune Signal, National Institute of Biomedical Innovation, Osaka 567-0085, Japan

[§]Department of Gastroenterology and Oncology, Institute of Health Biosciences, The University of Tokushima Graduate School, Tokushima 770-0855, Japan

Supporting Information

ABSTRACT: Sialylation is one of the most important types of glycosylation involved in carcinogenesis and establishment of cancer stemness. We previously showed that increased sialylation is a characteristic glycan change in cancer stem cells (CSCs) from hepatocellular carcinoma. However, the identities of glycoproteins targeted for sialylation remain unknown. In the present study, we identified glycoproteins targeted for sialylation in doxorubicin (DXR)-treated hepatocarcinoma cell line, Huh7, using glycoproteomic analyses. Since CSCs constitute a small subset of cells within carcinoma cell lines, it is difficult to identify sialylated proteins using general glycoproteomic strategies. It is known that treatment with anticancer drug can condense CSCs, we used DXR to concentrate CSCs. In DXR-treated Huh7 cells, isobaric tag for relative and absolute quantitation (iTRAQ) analysis identified 17 sialylated glycoproteins. Most of the identified glycoproteins were cancer-associated proteins. Furthermore, two proteins of approximately 70 kDa were detected using *Sambucus sieboldoana* agglutinin (SSA) blot analysis and identified as beta-galactosidase and alpha-2-HS-glycoprotein (fetuin-A) by SSA precipitation followed by liquid chromatography-tandem mass spectrometry analyses. Sialylation levels of fetuin-A were increased in DXR-treated Huh7 cell lysates. These changes in sialylation of glycoproteins might be involved in the establishment of cancer stemness.

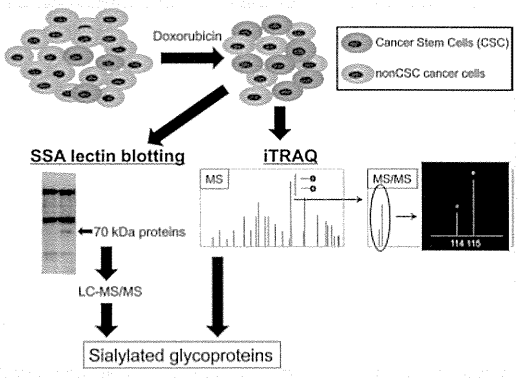

KEYWORDS: *sialylation, cancer stem cells, doxorubicin, hepatoma, glycoproteomics*

INTRODUCTION

A growing body of evidence suggests that tumors are frequently composed of heterogeneous cell types and that tumor initiation and growth are driven by a small subset of cells, termed cancer stem cells (CSCs), or tumor-initiating cells.[1−3] Several lines of research have indicated that CSCs can be preferentially resistant to many current therapies, including various chemotherapeutic agents and radiation treatment.[4−7] Thus, therapeutic strategies that effectively target CSCs could have a major impact on cancer patient survival. There are many reports on CSC markers, which include CD13,[8] CD44,[9,10] epithelial cell adhesion molecule (EpCAM),[11] and CD133.[9,12,13] These CSC markers have been used for identifying or concentrating CSCs in each type of cancer. It is unknown whether pure CSCs or whether heterogeneous populations containing CSC-like cells, should be targets for therapeutic strategies. Glycans are often attached to proteins and lipids on the cell surface and structurally and functionally modify these molecules. Glycans consist of several kinds of monosaccharides and show great structural diversity. Research in the field of glycobiology has revealed diverse and complex biological roles for these glycans.[14] The structures and amounts of glycans present on the cell surface change dramatically during development and differentiation.[15] We have recently reported that sialylated glycans are useful markers for CSC-like cells in hepatoma cell lines.[16] Glycomic analysis using a lectin microarray showed marked binding of *Sambucus sieboldoana* agglutinin (SSA) to a $CD133^+CD13^+$ cell subpopulation within hepatoma cell lines. SSA lectin recognizes α2, 6-sialic acid.[16] Sialic acid is one of the building blocks of glycans and is generally found at the outermost ends of the glycan chains of glycoproteins and glycolipids. Thus, sialic acid is associated with many physiological and pathological events, including binding to infectious pathogens, regulation of immune responses, and tumor malignancy.[17] In particular, the alteration of sialic acid moieties is associated with cancer cell behavior, such as invasiveness and metastasis.[18−23] Glycan changes are involved in development and differentiation, and sialic acid is one of the most important glycosylations involved in these processes.[24]

Special Issue: Proteomics of Human Diseases: Pathogenesis, Diagnosis, Prognosis, and Treatment

Received: May 1, 2014

In terms of glycoproteomic analyses, the identification of target proteins for each characteristic oligosaccharide structure is very important.[25] However, using the conventional strategy, which involves pooling and concentrating the CSC fraction using CD markers and lectins, it was not easy to obtain appropriate amounts of proteins for glycomic analyses. In general, CSC or CSC-like cells are resistant to anticancer drug treatment. For example, a CD133 and SSA double-positive population was resistant to several kinds of anticancer drug treatments such as 5-fluorouracil (5-FU) (Supplementary Figure 1). Hermann et al. also showed that the number of CD133-positive cells increased in human pancreatic cancer cells treated with gemcitabine.[26] These results suggest that short-term treatment with anticancer drugs can be used to easily concentrate CSCs. Among emerging proteomic technologies, isobaric tags for relative and absolute quantitation (iTRAQ) is a shotgun-based technique, which allows the concurrent identification and relative quantification of hundreds of proteins from different biological samples in a single experiment.[27,28] Whereas iTRAQ analysis leads to a more comprehensive analysis of sialylated proteins, the SSA lectin precipitation technique followed by liquid chromatography–tandem mass spectrometry (LC–MS/MS) analysis allows for protein enrichment, which aids in the identification of specific target proteins.

In the present study, we investigated characteristic glycan structures in the doxorubicin (DXR)-treated human hepatoma cell line Huh7, and further identified their target glycoproteins using iTRAQ and SSA lectin precipitation followed by LC–MS/MS. In addition, the expression levels of these proteins were confirmed using Western blotting, and their biological significance in CSC functions is discussed.

MATERIALS AND METHODS

Cell Culture and Cell Treatments

The human hepatoma cell line Huh7 was obtained from American Type Culture Collection (ATCC, Manassas, VA, USA) and cultured in RPMI 1640 (Sigma, St. Louis, MO, USA) medium containing 10% fetal bovine serum (Invitrogen, Carlsbad, CA, USA), supplemented with 100 units/mL penicillin G and 100 μg/mL streptomycin in a 37 °C incubator under a humidified atmosphere containing 5% CO_2. The cells were seeded into 100 mm dishes at 1×10^6 cells/dish. After 6 h, doxorubicin (DXR) (Sigma) was added to the culture medium (5 μg/mL). The cells were harvested after 48 h of exposure to DXR, and the culture media were harvested as conditioned media for the following analyses.

Lectin Microarray

Patterns of oligosaccharide structures in Huh7 cells treated with or without DXR were investigated by means of evanescent-field fluorescence-assisted lectin microarray. Forty-five types of lectins were immobilized on a glass slide in triplicate. The procedure has been described in detail, previously.[29] Briefly, total cellular proteins in phosphate buffered saline (PBS) containing 1% Triton X-100 were labeled with Cy3-succinimidyl ester (GE Healthcare, Chalfont St. Giles, U.K.) at room temperature (RT) for 1 h in the dark. Excess reagent was removed by gel filtration chromatography. The resultant Cy3-labeled protein solution was applied to a lectin microarray. After incubation at 20 °C for 15 h, the glass slide was scanned with an evanescent-field fluorescence scanner, GlycoStation (GP Biosciences Ltd., Kanagawa, Japan). All of the data were analyzed using Array Pro Analyzer version 4.5 (Media Cybernetics, Inc., Bethesda, MD, USA). The net intensity value for each spot was calculated by subtracting the background value. The signal intensity value for each lectin was expressed as the average of the net intensity values for three spots. The signal from wheat germ agglutinin (WGA) was used to normalize the signal intensity of each lectin because binding to WGA lectin was relatively stable and similar using different cell types.

Mass Spectrometric Analysis

NanoLC–MS/MS analyses were performed on LTQ-Orbitrap XL (Thermo Fisher Scientific, Waltham, MA) equipped with nano-ESI source and coupled to Paradigm MG4 pump (Michrom Bioresources, Auburn, CA) and autosampler (HTC PAL, CTC Analytics, Zwingen, Switzerland). Peptide mixtures were separated on MagicC18AQ column (100 mm × 150 mm, 3.0 μm particle size, 300 Å, Michrom Bioresources) with a flow rate of 500 nL/min. A linear gradient of 5–30% B in 80 min, 30–95% B in 10 min, and 95% B for 4 min and finally decreased to 5% B was employed (A = 0.1% formic acid in 2% acetonitrile; B = 0.1% formic acid in 90% acetonitrile). Intact peptides were detected in the Orbitrap at 30,000 resolution. Up to three CID and HCD spectra were acquired in a data-dependent acquisition mode following each full scan (m/z, 400–1500). The mass spectrometer was operated in positive ion mode.

Preparation of Labeled Peptides for Isobaric Tags for Relative and Absolute Quantitation (iTRAQ) Analysis

Each protein sample (adjusted to 4.1 mg) was digested with 50 μg of Trypsin-TPCK Solution (Applied Biosystems, Framingham, MA, USA) at 37 °C overnight and sialylated proteins were isolated using *Sambucus sieboldiana* agglutinin (SSA) covalently linked to agarose beads (SSA-agarose) (J-Oil Mills, Inc., Tokyo, Japan). After applying to an SSA-agarose column, each sample was incubated for 6 h at 4 °C. The SSA-Agarose column was washed with 1 mL of 50 mM Tris HCl [pH 7.4] buffer five times. Bound peptides were eluted from the SSA-Agarose column using 1 mL of the elution buffer (0.2 M lactose) three times. The eluted samples were deglycosylated with glycopeptidase F. Deglycosylated peptides were desalted and labeled with iTRAQ reagents (Applied Biosystems) according to the manufacturer's instructions. Proteins from Huh7 cells, treated with or without DXR and eluted from SSA agarose, were labeled with iTRAQ reagents 114 and 115, respectively. All labeled peptide samples were mixed and fractionated as described previously.[30]

iTRAQ Data Analysis

Protein identification and quantification for iTRAQ analysis was carried out using Proteome Discoverer v.1.3 (Thermo Fisher Scientific) using the MASCOT algorithm against Swiss-Prot protein database (Swiss-Prot_2012_06 536,489 entries). Taxonomy was set to *Homo sapiens* (20,312 entries). Search parameters for peptide and MS/MS mass tolerance were 10 ppm and 0.8 Da, respectively, with allowance for two missed cleavages made from the trypsin digest. Carbamidomethylation (Cys) and iTRAQ4plex (Lys, N-terminal) were specified as static modifications, whereas deamidation (Asn, Gln), iTRAQ4plex (Tyr), and oxidation (Met) were specified as dynamic modifications in the database search. When deamidation of Asn were detected, the amino acids were considered as glycan binding site because glycopeptidase F treatment convert glycosylated Asn residue to Asp. Mascot results were filtered with the integrated Percolator based filter using a false discovery rate <1% (based on PSMs). Relative protein abundances were calculated using the ratio of iTRAQ reporter ion in the MS/MS scan. List of the

dx.doi.org/10.1021/pr5004399 | J. Proteome Res. XXXX, XXX, XXX–XXX

glycoproteins identified in iTRAQ analysis was represented in Supplementary Table 1.

Protein Identification by Mass Spectrometry

The gels were stained with the Silver Stain MS kit according to the manufacturer's instruction (WAKO Pure Chemical Industries, Ltd., Osaka, Japan). Protein spots in a silver-stained gel, corresponding to positive spots on Western blot membranes, were excised from the gel and digested in gel according to a previously described method,[31,32] using sequencing grade modified trypsin (Promega, Inc., Madison, WI). Digested peptides were then extracted with 5% TFA in acetonitrile (acetonitrile/DW 50:45), sonicated for 5 min and concentrated by evaporation. Dried peptides were dissolved in 0.1% TFA (v/v) and 2% acetonitrile (v/v) for subsequent LC–MS/MS analysis. NanoLC–MS/MS analyses were performed on a LTQ-Orbitrap XL mass spectrometer (Thermo Fisher Scientific) equipped with a nano-ESI source (AMR) and coupled to a Paradigm MG4 pump (Michrom Bioresources) and an autosampler (HTC PAL, CTC Analytics). A spray voltage of 1800 V was applied. The peptide mixture was separated on a Magic C18AQ column (100 μm × 150 mm, 3.0 μm particle size, 300 Å, Michrom Bioresources) with a flow rate of 500 nL/min. The linear gradient of 5% to 45% B in 30 min, 45% to 95% B in 0.1 min, and 95% B for 2 min and finally decreased to 5% B was employed (A = 0.1% formic acid in 2% acetonitrile; B = 0.1% formic acid in 90% acetonitrile). Intact peptides were detected in the Orbitrap at 60,000 resolutions. For LC–MS/MS analysis, 6 precursor ions were selected for subsequent MS/MS scans in a data-dependent acquisition mode following each full scan (m/z, 350–1500). A lock mass function was used for the LTQ-Orbitrap to obtain constant mass accuracy during gradient analysis. Peptides and proteins were identified by means of automated database search using Proteome Discoverer v.1.3 (Thermo Fisher Scientific) against human of Swiss-Prot protein database (Swiss-Prot_2012_06) with a precursor mass tolerance of 10 ppm, a fragment ion mass tolerance of 0.8 Da, and strict trypsin specificity, allowing for up to two missed cleavages. Carbamidomethylation of cysteine was set as a fixed modification, and oxidation of methionines was allowed as dynamic modifications. Raw data of MS/MS analysis was represented in Supplementary Figure 2.

Lectin Blot Analysis

Huh7 cells were quickly harvested from a 100 mm dish in ice-cold PBS. After precipitation by centrifugation at 2000 rpm for 5 min at 4 °C, the cells were resuspended in TNE buffer (10 mM Tris-HCl [pH 7.8], 1% NP40, 1 mM EDTA, and 0.15 M NaCl) containing a protease inhibitor cocktail (Roche, Mannheim, Germany) and then placed on ice for 30 min to allow solubilization. Samples were then centrifuged at 15,000 rpm for 15 min at 4 °C, and the supernatants were collected as cell lysates. Samples were quantitated using a bicinchoninic acid (BCA) assay kit (Pierce, Rockford, IL, USA).

In each experiment, duplicate samples were subjected to 8% sodium dodecyl sulfate polyacrylamide gel electrophoresis (SDS-PAGE) under reducing conditions. One gel was subjected to Coomassie Brilliant Blue (CBB) R-250 staining and another was transferred to a polyvinyl difluoride (PVDF) membrane (Millipore Corp., Billerica, MA, USA) for lectin blot analysis, using SSA, *Leukoagglutinating phytohemagglutinin* (L4-PHA), *Aleuria aurantia* lectin (AAL), and *Datura stramonium* (DSA). After blocking with PBS containing 3% bovine serum albumin (BSA) overnight at 4 °C, each membrane was incubated in 1:2500–1:10000 diluted biotinylated SSA, L4-PHA, AAL, and DSA (J-Oil Mills, Inc., Tokyo, Japan) for 20 min at RT. The membranes were then washed three times with Tris-buffered saline containing 0.05% Tween-20 (TBST) (pH 7.4) and incubated with 1:2500 diluted avidin–peroxidase conjugates (ABC kits, Vector Res. Corp., Burlingame, CA, USA) for 20 min at RT. The membrane was again washed three times with TBST and then developed using an enhanced chemiluminescence system, Immobilon Western (Millipore), according to the manufacturer's protocol.

Immunoblot Analysis

Cell lysates and conditioned media were subjected to 8% SDS-PAGE under reducing conditions and then transferred to a PVDF membrane (Millipore). After blocking with PBS containing 5% skim milk for 1 h at RT, each membrane was incubated overnight at 4 °C with the following primary antibodies diluted 1:1000–1:5000: anti-HYOU1 (Abnova, Taipei, Taiwan), anti-P4HA1 (Abnova, Taipei City, Taiwan), anti-LAMP1 (Abcam Inc., Cambridge, MA, USA), anti-LAMP2 (Santa Cruz Biotechnology Inc., Santa Cruz, CA, USA), antibeta-galactosidase (Santa Cruz Biotechnology), antifetuin-A (Santa Cruz Biotechnology), or anti-β-actin (Cell Signaling, Beverly, MA, USA) for 60 min at RT. The dilution ratios for these antibodies ranged from 1:1000 to 1:5000. The membranes were then washed three times with Tris-buffered saline containing 0.05% Tween-20 (TBST) (pH 7.4) and incubated with 1:5000 diluted horseradish peroxidase conjugated with the appropriate secondary antibody for 30 min at RT. The membranes were again washed three times and developed using an Immobilon Western (Millipore).

Lectin Precipitation

Extracted protein (100 μg) was incubated with 40 μL of SSA-agarose overnight with shaking at 4 °C. Precipitated proteins were washed in 50 mM Tris HCl [pH 7.4] and then boiled in SDS sample buffer. Ten microliters of precipitated proteins were subjected to 8% SDS-PAGE. The gel was stained with Silver Stain MS Kits (Wako, Osaka, Japan). Protein bands were excised from the gel and digested with sequencing grade trypsin (Promega) as described previously.[33]

Neuraminidase/*N*-Glycanase Treatments

The extracted proteins (100 μg) were incubated overnight at 37 °C with 200 mU/mL of neuraminidase (Roche, Nutley, NJ, USA) in 50 mM AcOH buffer [pH 5.5] containing 4 mM $CaCl_2$ and 100 μg/mL BSA. In addition, 100 μg of the extracted proteins were incubated with glycopeptidase F (Takara Bio Inc., Otsu, Japan) according to the manufacturer's protocol. The cell lysates were subsequently boiled in SDS-PAGE sample buffer, electrophoresed on 8% SDS PAGE, and then transferred onto a PVDF membrane (Millipore). After blocking with TBST containing 5% skim milk at 4 °C overnight, Western blot analysis for fetuin-A was performed using antifetuin-A antibody.[34] Briefly, 1:5000 diluted antifetuin-A was incubated in TBST buffer containing 5% skim milk for 1 h at RT. After washing the membrane three times with TBST, it was incubated for 1 h at RT with the secondary antibody, horseradish peroxidase-conjugated antirabbit-IgG (Promega), diluted 1:5000. It was again washed three times and developed with an Immobilon Western (Millipore).

Immunofluorescence Confocal Microscopy

Huh7 cells were seeded in 35 mm dishes at 3 × 10^5 cells/dish. After 6 h, DXR was added to the culture medium (5 μg/mL). After 48 h of exposure to DXR, cells were washed once in PBS

dx.doi.org/10.1021/pr5004399 | J. Proteome Res. XXXX, XXX, XXX–XXX

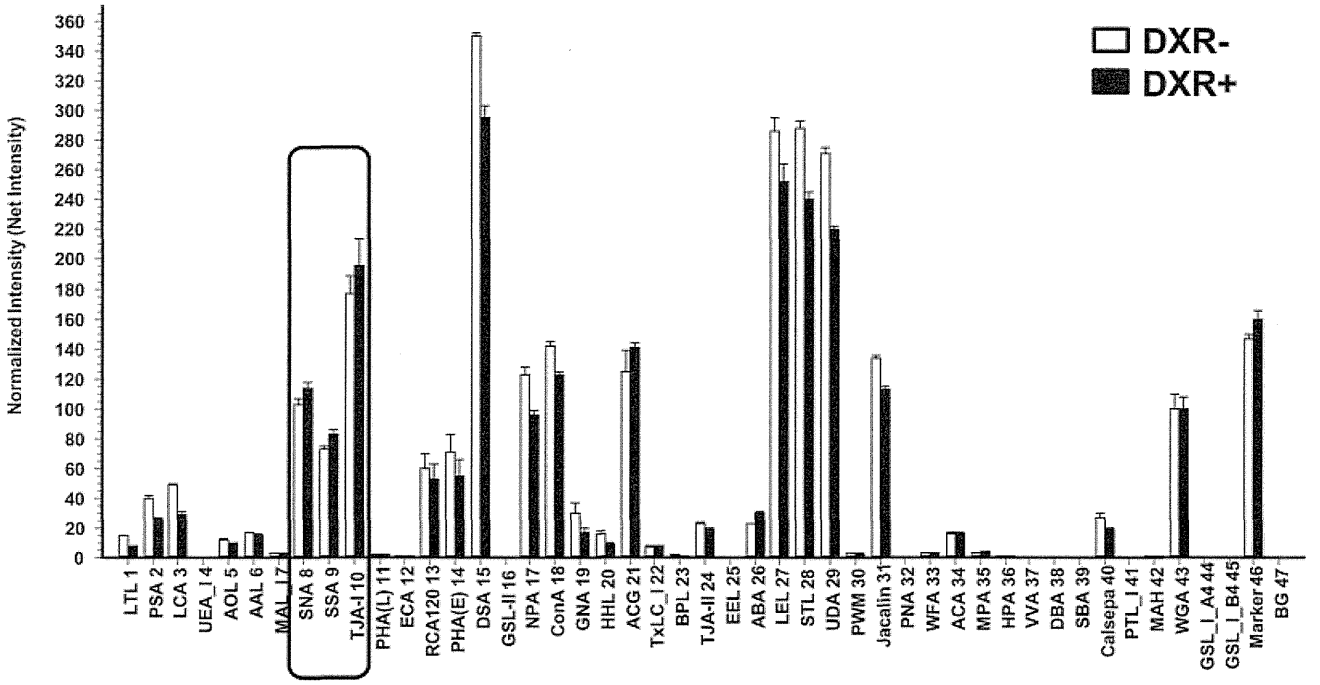

Figure 1. Lectin microarray analysis. Total cellular proteins of Huh7 cells treated with or without doxorubicin were analyzed three times using lectin microarray. Twenty-five nanogram aliquots of Cy3-labeled proteins were applied to each lectin microarray. The fluorescence intensity of each lectin was normalized to the intensity of WGA staining. All data are represented as mean ± standard deviations (SD). The Wilcoxon test was used to assess any significant differences in variables. There were significant increases in the intensities of SNA, SSA, and TJA-1 after doxorubicin treatment (DXR+) compared with the intensities in the absence of doxorubicin treatment (DXR−) ($P < 0.05$).

Table 1. Expression Profile of Sialylated Proteins in Doxorubicin-Treated Huh7 Cells, Obtained from iTRAQ Analysis

Swiss-Prot accession number	sequence	description	gene symbol	site	115/114	115/114 count	115/114 variability [%]
Q9Y4L1	VFGSQNLTTVK	hypoxia up-regulated protein 1	*HYOU1*	N515	7.137	1	
P13674	DMSDGFISNLTIQR	prolyl 4-hydroxylase subunit alpha-1	*P4HA1*	N367	4.857	1	
P11279	SGPKNMTFDLPSDATVVLNR	lysosome-associated membrane glycoprotein 1	*LAMP1*	N562, N76	3.796	1	
O60568	SAEFFNYTVR	procollagen-lysine, 2-oxoglutarate 5-dioxygenase 3	*PLOD3*	N63	2.848	1	
O60568	EQYIHENYSR	procollagen-lysine, 2-oxoglutarate 5-dioxygenase 3	*PLOD3*	N548	2.347	1	
P11142	VEIIANDQGNR	heat shock cognate 71 kDa protein	*HSPA8*	N31	2.152	1	
P16278	NNVITLNITGK	beta-galactosidase	*GLB1*	N458, N464	1.963	1	
P11279	NMTFDLPSDATVVLNR	lysosome-associated membrane glycoprotein 1	*LAMP1*	N62, N76	1.890	1	
Q92508	ELYNGTADITLR	piezo-type mechanosensitive ion channel component 1	*PIEZO1*	N2294	1.852	1	
P11279	ENTSDPSLVIAFGR	lysosome-associated membrane glycoprotein 1	*LAMP1*	N84	1.836	2	6.0
Q86VZ4	SSDNVSVTVLR	low-density lipoprotein receptor-related protein 11	*LRP11*	N291	1.806	2	8.6
P19022	SNISILR	cadherin-2	*CDH2*	N692	1.804	1	
P13473	AASTYSIDSVSFSYNTGDNTTFPDAEDK	lysosome-associated membrane glycoprotein 2	*LAMP2*	N257	1.699	1	
Q5ZPR3	TALFPDLLAQGNASLR	CD276 antigen	*CD276*	N104	1.697	1	
P11047	TLAGENQTAFEIEELNR	laminin subunit gamma-1	*LAMC1*	N1223	1.696	1	
Q5ZPR3	QLVHSFAEGQDQGSAYANR	CD276 antigen	*CD276*	N309	1.634	1	
P13473	VQPFNVTQGK	lysosome-associated membrane glycoprotein 2	*LAMP2*	N356	1.614	2	12.5
P56199	VYVYALNQTR	integrin alpha-1	*ITGA1*	N532	1.611	1	

and fixed with methanol for 10 min at −20 °C, followed by blocking with PBS containing 1% BSA for 1 h at RT. The cells were then incubated overnight at 4 °C with the mouse antifetuin-A antibody (Santa Cruz Biotechnology) and rabbit antialbumin

dx.doi.org/10.1021/pr5004399 | J. Proteome Res. XXXX, XXX, XXX−XXX

antibody (Rockland Immunochemicals, Gilbertsville, PA, USA). Fluorescein isothiocyanate (FITC)-conjugated SSA (J-Oil Mills, Inc., Tokyo, Japan) was incubated for 2 h at RT. Primary antibody binding was detected with Alexa-488 antimouse IgG or Alexa-546 antirabbit IgG (Invitrogen). Finally, the cells were washed three times for 2 min with PBS. Staining was evaluated using confocal microscopy.

Statistical Analysis

Statistical analyses were conducted using JMP Pro 10.0 software (SAS Institute Inc., Cary, NC, USA). Variables in lectin array analyses were expressed as the mean ± standard deviation (SD). The Wilcoxon test was used to assess any significant differences in variables. Differences were considered statistically significant at $P < 0.05$.

RESULTS

Glycan Profiling of Huh7 Cells Treated with or without DXR Using Lectin Microarray

First, we determined the DXR IC_{50} concentration in Huh7 cells treated with DXR for 48 h, using the WST assay (Nacalai Tesque, Kyoto, Japan) (data not shown). Huh7 cells were treated with the IC_{50} concentration of DXR (5 μg/mL) for 48 h, and then Cy3-labeled proteins derived from these cells were subjected to lectin microarray analysis (Figure 1). Interestingly, the intensities of three sialylated glycan-recognizing lectins (SNA, SSA, and TJA-1) among 43 lectins were significantly higher in DXR-treated cells than in untreated cells. This finding is very similar to that of our previous study, which demonstrated that hepatic CSCs (CD133 and CD13 double-positive Huh7 cells) highly expressed sialylated glycans.[16] In this previous study, we also demonstrated that SSA lectin could be used as a tool for isolating CSCs. Unexpectedly, binding to the lectins PSA and LCA was slightly decreased in DXR-treated cells. Both PSA and LCA lectins recognize α1−6 core fucosylation, which is involved in carcinogenesis. Changes in the branching formation of *N*-glycans, as judged by binding to L4-PHA lectin, were not observed in Huh7 cells treated with DXR.

Sialylated Protein Expression Profile of Huh7 Cells Treated with or without DXR

To identify target glycoproteins that show increased sialylation upon DXR treatment, iTRAQ analysis was performed. Total cell lysates from Huh7 cells treated with or without DXR were trypsinized and applied to a SSA-agarose column. Subsequently, captured sialylated glycopeptides were deglycosylated with glycopeptidase F and labeled with a specific isobaric iTRAQ reagent. A total of 191 proteins were identified with this analysis. Among these, we have listed glycoproteins that showed more than 1.6-fold expression in DXR-treated Huh7 cells as compared with that in DXR-untreated Huh7 cells (Table 1).

Western Blot Analysis of Glycoprotein Listed by iTRAQ Analysis

To further verify the changes in the glycoproteins listed in Table 1, we selected four proteins [hypoxia up-regulated protein 1 (HYOU1), prolyl 4-hydroxylase subunit alpha-1 (P4HA1), lysosomal-associated membrane glycoprotein 1 (LAMP1), and LAMP2], which are known to be abundantly glycosylated and associated with cancer, for validation using Western blotting (Figure 2). The expression levels of HYOU1 and P4HA1 showed no significant differences between Huh7 cells with or without DXR treatment. This indicates that the sialylation levels of these proteins increased with DXR treatment and total protein levels were not changed. In contrast, both LAMP1 and LAMP2 protein levels were slightly increased in DXR-treated Huh7 cells.

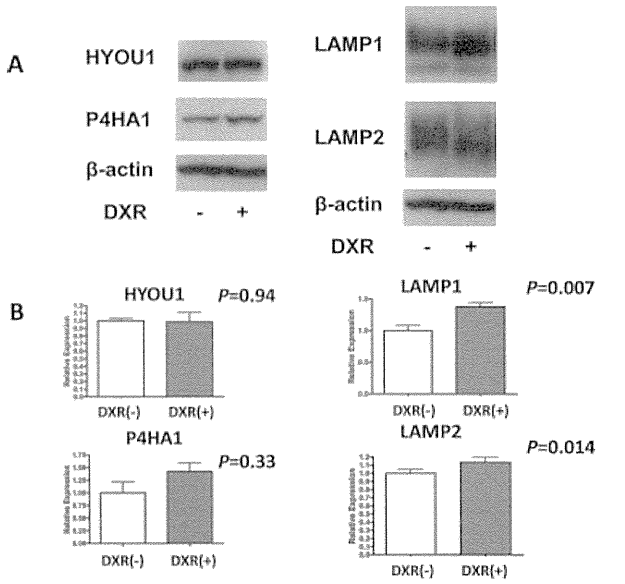

Figure 2. Western blot analyses of HYOU1, P4HA1, LAMP1, and LAMP2. (A) Twenty-five micrograms (HYOU1 and P4HA1), 10 μg (LAMP1 and β-actin), and 2.5 μg (LAMP2) of total cellular proteins were electrophoresed on 8% polyacrylamide gels, and Western blot analyses were performed. β-actin was used as the control. (B) Expression level of each protein band was determined by ImageJ64 software for three independent blots, and statistical analysis was performed by Wilcoxon test. Each result represented the mean ± SD.

Increase in Sialylation of 70 kDa Proteins in DXR-Treated Huh7 Cells

Next, we performed lectin blot analysis to determine changes in sialylation in each protein band in DXR-treated Huh7 cells. Very interestingly, dramatic increases in sialylation in approximately 70 kDa proteins were observed (Figure 3A). While other bands

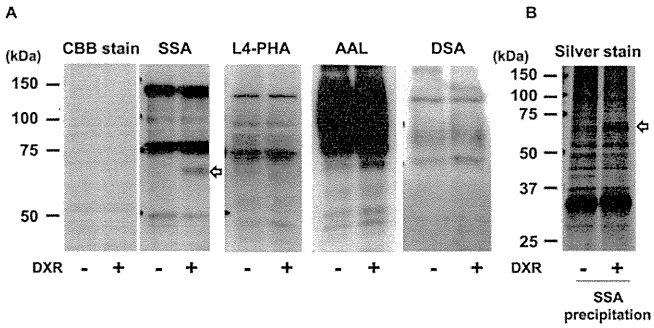

Figure 3. Lectin blot analyses and SSA precipitation of Huh7 cells treated with or without doxorubicin. (A) Lectin blot analyses using SSA, AAL, L4-PHA, and DSA. (B) Proteins were captured by SSA-agarose bead complexes, followed by 10% SDS-PAGE analysis with silver staining. The arrows indicate specifically sialylated bands. These data were results from 3−5 independent experiments.

in the SSA lectin blot were slightly increased or decreased in DXR-treated cells, the 70 kDa proteins were very prominent. Therefore, the protein levels of these 70 kDa proteins might be increased upon DXR treatment. Mechanisms that can increase sialylation in glycoproteins include increased branching, increased presence of Lewis structures, and extension of lactosamine structure repeats. L4-PHA, AAL, and DSA can recognize these glycan structures, respectively. Therefore, we examined these lectin blot analyses. The 70 kDa band was not

dx.doi.org/10.1021/pr5004399 | J. Proteome Res. XXXX, XXX, XXX−XXX

detected in other lectin blot analyses, although a significant increase was observed in AAL lectin blot analysis (Figure 3A). The increase in the intensity of the 70 kDa band in the DXR-treated cells in the AAL blot indicates an increased presence of Lewis structures in some glycoproteins. To capture this sialylated glycoprotein at 70 kDa, SSA precipitation was performed (Figure 3B). As shown in Figure 3B, approximately 70 kDa sialylated glycoproteins were identified using SSA-agarose precipitation followed by silver staining. Next, the 70 kDa protein spot was digested with trypsin, and the extracted peptides were analyzed using LC–MS/MS. The spectra thus acquired were searched against the Swiss-Prot database with the aid of the MASCOT search engine. In this manner, we identified five proteins as candidate sialylated glycoproteins (Table 2).

Table 2. Sialylated 70 kDa Proteins Identified by LC–MS/MS

Swiss-Prot accession no.	protein	peptide matching	protein coverage (%)
P16278	beta-galactosidase	12	11.23
P02765	alpha-2-HS-glycoprotein (fetuin-A)	8	5.45
Q02413	desmoglein-1	2	0.95
Q9NPR9	protein GPR108	2	2.03
P11279	lysosome-associated membrane glycoprotein 1	1	2.64

Evaluation of the 70 kDa Sialylated Proteins in DXR-Treated Huh7 Cells by Western Blot

To evaluate the 70 kDa sialylated proteins listed in Table 1, Western blotting was performed. Because of their large hit numbers in LC–MS/MS analysis, we focused on fetuin-A and beta-galactosidase. Although the protein expression of beta-galactosidase was slightly increased in DXR-treated Huh7 cells, the protein expression of beta-galactosidase obtained by SSA precipitation was much greater in DXR-treated Huh7 cells (Figure 4A). This result indicates that the sialylation levels of beta-galactosidase increased with DXR treatment. Next, Western blot analyses of alpha-2-HS-glycoprotein (fetuin-A) were performed. Although the protein expression of fetuin-A in total cell lysate was lower in DXR-treated Huh7 cells, the protein expression of fetuin-A obtained by SSA precipitation was significantly higher in DXR-treated Huh7 cells (Figure 4B). Furthermore, the molecular weight of fetuin-A was higher in DXR-treated Huh7 cells. These results indicate that oligosaccharide structures of fetuin-A are completely different between DXR-treated and untreated Huh7 cells. Additionally, the molecular weight of fetuin-A in the conditioned medium was almost the same between DXR-treated and untreated cells, which was consistent with the sialylated fetuin-A band (70 kDa) observed in cell lysates treated with DXR (Figure 4C). We found that sialylated fetuin (70 kDa) was barely observed in untreated cell lysate and almost all of the 70 kDa fetuin was secreted into the medium in the absence of DXR treatment. In order to determine whether the changes in molecular weight of fetuin-A were due to glycosylation/sialylation, the total cell lysates of DXR-treated and untreated Huh7 cells were incubated with 200 mU/mL neuraminidase, which specifically cleaves terminal sialic acid residues. A decrease of the molecular weight of fetuin-A was observed following neuraminidase treatment, suggesting that sialylation in fetuin-A was increased upon DXR treatment (Figure 4D). Next, to determine whether the changes in fetuin-A bands were dependent on N-glycosylation, cell lysates were treated with 20 mU/mL glycopeptidase F, which removes most complex type N-linked carbohydrates from glycoproteins. As expected, the fetuin-A band was decreased following this treatment (Figure 4D).

Localization of Fetuin-A in Huh7 Cells Treated with DXR

To examine the localization of fetuin-A in DXR-treated Huh7 cells, an immunofluorescence study was performed. Cells were stained with antifetuin-A antibody (Figure 5A,B), and anti-albumin antibody, which served as a nonglycosylated secretory protein control (Figure 5A) and SSA (Figure 5B). Although the expression of fetuin-A was lower in DXR-treated Huh7 cells than in untreated cells, colocalization of fetuin-A and albumin were observed in DXR-treated and untreated cells. In contrast, the localization of SSA changed dramatically in DXR-treated cells (Figure 5B). The localization of these signals was altered in DXR-treated cells from a perinuclear pattern to a scatter pattern in the cytoplasm. SSA and fetuin-A were not colocalized in DXR-untreated cells, but a few DXR-treated cells showed colocalization of SSA and fetuin-A (Figure 5B).

DISCUSSION

In the present study, to identify target glycoproteins for SSA lectin, we first used iTRAQ systems with SSA-agarose capture. However, the amounts of cellular proteins that could be isolated using CD133 antibody and SSA lectin were too small for proteomic analyses. Therefore, we used the anticancer drug DXR. Theoretically, treatment with DXR at its IC_{50} can concentrate CSCs. Lectin array analyses showed increased binding to SSA, SNA, and TJA-1 in DXR-treated Huh7 cells. Similar results were obtained in CD133 and CD13 double-positive CSCs derived from Huh7 cells.[16] These findings suggest that Huh7 cells treated with DXR display similar characteristics to CSCs. SSA, SNA, and TJA-1 recognize terminal α2, 6-sialic acid residues. We speculate that this increased sialylation in DXR-treated Huh7 cells might have potential benefits for the survival of anticancer drug-treated cells. To identify those glycoproteins that are targets for sialylation, iTRAQ analysis was performed. Of the 19 candidate glycoproteins we identified, concentration of HYOU1 was much greater than those of the other glycoproteins. HYOU1 plays an important role in hypoxia/ischemia and angiogenesis. HYOU1 is overexpressed in invasive breast cancer, and its overexpression appears to be associated with poor prognosis.[35] A high score in iTRAQ analyses using SSA agarose capture may indicate one of two possibilities: an increase in the glycoprotein level itself or an increase in sialic acid levels in a specific glycoprotein. Protein levels remain unchanged in the case of HYOU1 (Figure 2). Although we would have liked to perform immunoprecipitation followed by SSA lectin blotting, the antibody for immunoprecipitation was not available. We predict that sialic acid increases in HYOU1 in DXR-treated Huh7 cells. The next high score in iTRAQ analysis was that of P4HA1. P4HA1 plays a central role in collagen synthesis. P4HA1 has also been shown to be expressed in hepatocellular carcinoma tissue. In contrast, the protein expression levels of LAMP1 and LAMP2 were increased with DXR treatment. LAMP1 and LAMP2 are localized primarily in the periphery of lysosomes and are recognized as major constituents of the lysosomal membrane.[36] It is well-known that these molecules are among the most heavily glycosylated cellular proteins, with approximately 50% of their mass being carbohydrates. Therefore, these proteins could be captured by an SSA-agarose column and detected using iTRAQ analysis. Since these 4 glycoproteins are associated with cancer progression as well as metastasis, increases in sialic acid content

dx.doi.org/10.1021/pr5004399 | J. Proteome Res. XXXX, XXX, XXX–XXX

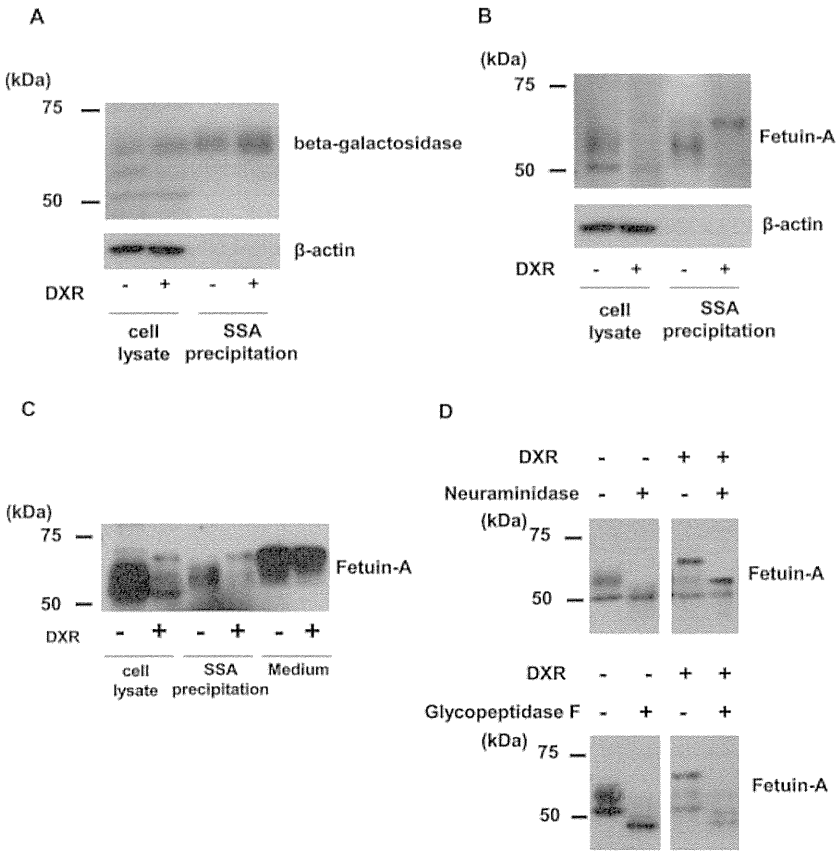

Figure 4. Evaluation of 70 kDa sialylated proteins in Huh7 cells treated with doxorubicin with Western blotting. (A) Ten micrograms of cell lysate and total cellular proteins obtained from lectin precipitation (50 μg) were electrophoresed on 8% acrylamide gels, and Western blot analyses of beta-galactosidase were performed. (B) Western blotting analysis of fetuin-A was performed. (C) Western blotting analysis of fetuin-A from Huh7 cell lysates (30 μg) and conditioned media (1 μL) in the presence or absence of DXR treatment. (D) Cell lysates were treated with neuraminidase or glycopeptidase F at 37 °C overnight. The lysates were then subjected to 8% SDS-PAGE analysis. These data were results from 3 independent experiments.

in these proteins can change biological characteristics, including cancer stemness.

Next, we conducted an SSA lectin blot analysis to determine total/partial increases in sialic acid content in DXR-treated Huh7 cells. Surprisingly, proteins approximately 70 kDa in mass were specifically sialylated. From LC–MS/MS analyses, we identified five proteins that were not identified by iTRAQ analysis, with the exception of LAMP1. Fetuin-A (predicted molecular weight: 38 kDa), GPR108 (predicted molecular weight: 60 kDa), LAMP1 (predicted molecular weight: 45 kDa), and LAMP2 (predicted molecular weight: 45 kDa) are abundantly glycosylated. In our study, 70 kDa fetuin-A was heavily sialylated. Therefore, the band sizes of fetuin-A, GPR108, LAMP1, and LAMP2 were heavier than the predicted molecular weights. In addition, the predicted size of beta-galactosidase is about 116 kDa, but the alternatively spliced variant of beta-galactosidase was reported to be about 67 kDa.[37] Desmoglein-1 (predicted molecular weight: 112 kDa) would be cleaved by DXR-activated proteases. The reason why these proteins were not identified by iTRAQ is likely due to the analysis method of iTRAQ. Because proteins are cleaved into peptides in iTRAQ analysis, the steric structures of each protein is not reflected in iTRAQ analysis. In contrast, the steric structures of each protein and the site of *N*-glycan attachment are necessary in SSA precipitation analysis. These differences between iTRAQ and SSA precipitation are likely the reason for the different results seen in our study.

In LC–MS/MS analysis, we focused on beta-galactosidase and fetuin-A because of their predominantly large hit numbers. Beta-galactosidase (lysosomal hydrolase) cleaves the terminal beta-galactose from glycoconjugates. It is reported that anticancer drug treatment induces a senescence-like phenotype, and senescent cells are characterized by the appearance of senescence-associated beta-galactosidase.[38] Therefore, increases in sialic acid in beta-galactosidase in DXR-treated Huh7 cells are very interesting. Another glycoprotein, identified as a 70 kDa sialylated glycoprotein, was fetuin-A. Fetuin-A is well-known as a heavily sialylated glycoprotein with both N-linked and O-linked carbohydrate side chains.[39,40] Although various previous reports have discussed the biological functions of fetuin-A,[41,42] no studies have demonstrated differences in fetuin-A functions due to glycosylation differences. Asialofetuin-A is well-known to bind easily to galectin-3, while sialylated fetuin (sialofetuin) is reported to have no binding ability to galectin-3.[43,44] These biological differences would contribute to the functional diversity of variously glycosylated fetuin-A.

Neuraminidase treatment decreases the molecular weight of fetuin-A in DXR-treated Huh7 cells, and the lowered molecular weight was consistent with that of fetuin-A in DXR-untreated Huh7 cells, suggesting that fetuin-A was heavily sialylated in DXR-treated Huh7 cells. The question arises as to why this sialylated fetuin-A was not secreted into the conditioned medium. Therefore, we performed immunocytochemical analysis using confocal microscopy. Most of the fetuin-A was colocalized with albumin in DXR-treated cells compared to untreated cells, indicating that the secreted proteins were in the same endosome as during DXR treatment. A previous study

dx.doi.org/10.1021/pr5004399 | J. Proteome Res. XXXX, XXX, XXX–XXX

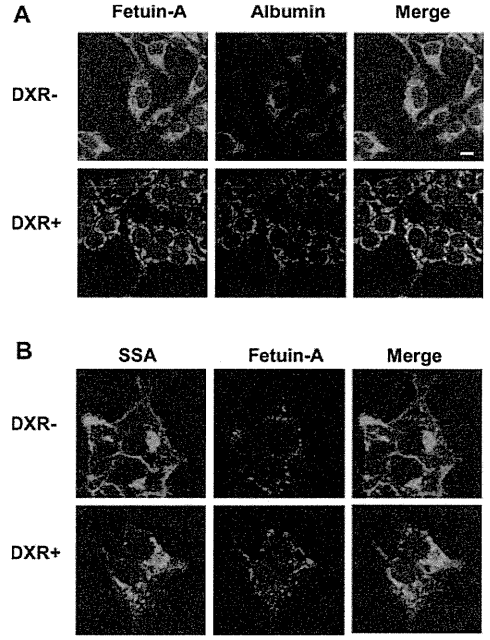

Figure 5. Localization of fetuin-A in Huh7 cells treated with doxorubicin. Immunocytochemical analyses were performed in Huh7 cells treated with or without DXR. After fixation of the cells, staining signals were visualized by laser scanning confocal microscopy. (A) Fetuin-A was visualized by Alexa-488-labeled immunostaining (green), albumin was visualized by Alexa-546-labeled immunostaining (red). (B) SSA was visualized by FITC labeling (green), and fetuin-A was visualized by Alexa-546-labeled immunostaining (red). The magnification is ×120. The bar indicates 10 μm. These data were results from 3 independent experiments.

showed that DXR induced apoptosis at a high dose (IC_{90}) but induced autophagy at a low dose (IC_{50}).[45] However, fetuin-A was not located in either the lysosome or the autophagosome (data not shown). Next we examined immunostaining of SSA to detect sialylated proteins. Surprisingly, SSA staining was dramatically changed, and a few cells showed colocalization of fetuin-A and SSA in DXR-treated cells. These results indicate that a small amount of sialylated fetuin-A remained inside the cell in DXR-treated cells. In general, fetuin-A is known as a highly sialylated serum protein.[46] Most sialylated fetuin-A might be promptly secreted to the conditioned medium (Figure 4C). In contrast, a small amount of sialylated fetuin-A remained inside the cell in DXR-treated cells. Further studies should be performed using sialyltransferase knockout or knockdown cells to evaluate the relationship between sialylation and the localization of glycoproteins, especially that of fetuin-A in anticancer drug treated cells. Since sialylation is a glycomarker for stem cells,[16,47] changes in the localization of sialylated proteins in CSCs might be involved in stem cell biology.

■ ASSOCIATED CONTENT

Supporting Information

Proliferation of CD133 positive Huh7 cells (SSA positive (+) or negative (−)) under 5-FU treatment. Raw data of MS/MS analysis. List of the glycoproteins identified in iTRAQ analysis. This material is available free of charge via the Internet at http://pubs.acs.org.

■ AUTHOR INFORMATION

Corresponding Author

*(E.M.) Tel/Fax: +81-6-6879-2590. E-mail: emiyoshi@sahs.med.osaka-u.ac.jp.

Notes

The authors declare no competing financial interest.

■ ACKNOWLEDGMENTS

This study was supported by a Grant-in-Aid for Scientific Research (A), No. 21249038, from the Japan Society for the Promotion of Science, and partially supported as a research program of the Project for Development of Innovative Research on Cancer Therapeutics (P-Direct), Ministry of Education, Culture, Sports, Science and Technology of Japan.

■ ABBREVIATIONS

CSCs, cancer stem cells; DXR, doxorubicin; SSA, *Sambucus sieboldiana* agglutinin; SNA, *Sambucus nigra* lectin; TJA-1, *Tricosanthes japonica* agglutinin-1; PSA, *Pisum sativum* agglutinin; LCA, *Lens culinaris* agglutinin; WGA, Wheat germ agglutinin; L4-PHA, *Leukoagglutinating phytohemagglutinin*; AAL, *Aleuria aurantia* lectin; DSA, *Datura stramonium agglutinin*; iTRAQ, isobaric tags for relative and absolute quantitation; HYOU1, hypoxia up-regulated protein 1; P4HA1, prolyl 4-hydroxylase subunit alpha-1; LAMP1, lysosomal-associated membrane glycoprotein 1

■ REFERENCES

(1) Reya, T.; Morrison, S. J.; Clarke, M. F.; Weissman, I. L. Stem cells, cancer, and cancer stem cells. *Nature* **2001**, *414* (6859), 105–11.

(2) Ailles, L. E.; Weissman, I. L. Cancer stem cells in solid tumors. *Curr. Opin. Biotechnol.* **2007**, *18* (5), 460–6.

(3) Mertins, S. D. Cancer stem cells: a systems biology view of their role in prognosis and therapy. *Anticancer Drugs* **2014**, *25* (4), 353–67.

(4) Dean, M.; Fojo, T.; Bates, S. Tumour stem cells and drug resistance. *Nat. Rev. Cancer* **2005**, *5* (4), 275–84.

(5) Bao, S.; Wu, Q.; McLendon, R. E.; Hao, Y.; Shi, Q.; Hjelmeland, A. B.; Dewhirst, M. W.; Bigner, D. D.; Rich, J. N. Glioma stem cells promote radioresistance by preferential activation of the DNA damage response. *Nature* **2006**, *444* (7120), 756–60.

(6) Malik, B.; Nie, D. Cancer stem cells and resistance to chemo and radio therapy. *Front. Biosci., Elite Ed.* **2012**, *4*, 2142–9.

(7) Baumann, M.; Krause, M.; Thames, H.; Trott, K.; Zips, D. Cancer stem cells and radiotherapy. *Int. J. Radiat. Biol.* **2009**, *85* (5), 391–402.

(8) Haraguchi, N.; Ishii, H.; Mimori, K.; Tanaka, F.; Ohkuma, M.; Kim, H. M.; Akita, H.; Takiuchi, D.; Hatano, H.; Nagano, H.; Barnard, G. F.; Doki, Y.; Mori, M. CD13 is a therapeutic target in human liver cancer stem cells. *J. Clin. Invest.* **2010**, *120* (9), 3326–39.

(9) Zhu, Z.; Hao, X.; Yan, M.; Yao, M.; Ge, C.; Gu, J.; Li, J. Cancer stem/progenitor cells are highly enriched in CD133+CD44+ population in hepatocellular carcinoma. *Int. J. Cancer* **2010**, *126* (9), 2067–78.

(10) Yang, Z. F.; Ho, D. W.; Ng, M. N.; Lau, C. K.; Yu, W. C.; Ngai, P.; Chu, P. W.; Lam, C. T.; Poon, R. T.; Fan, S. T. Significance of CD90+ cancer stem cells in human liver cancer. *Cancer Cell* **2008**, *13* (2), 153–66.

(11) Al-Hajj, M.; Wicha, M. S.; Benito-Hernandez, A.; Morrison, S. J.; Clarke, M. F. Prospective identification of tumorigenic breast cancer cells. *Proc. Natl. Acad. Sci. U.S.A.* **2003**, *100* (7), 3983–8.

(12) Kojima, K.; Musch, M. W.; Ren, H.; Boone, D. L.; Hendrickson, B. A.; Ma, A.; Chang, E. B. Enteric flora and lymphocyte-derived cytokines determine expression of heat shock proteins in mouse colonic epithelial cells. *Gastroenterology* **2003**, *124* (5), 1395–407.

(13) Ding, W.; Mouzaki, M.; You, H.; Laird, J. C.; Mato, J.; Lu, S. C.; Rountree, C. B. CD133+ liver cancer stem cells from methionine adenosyl transferase 1A-deficient mice demonstrate resistance to transforming growth factor (TGF)-beta-induced apoptosis. *Hepatology* **2009**, *49* (4), 1277–86.

(14) Fuster, M. M.; Esko, J. D. The sweet and sour of cancer: glycans as novel therapeutic targets. *Nat. Rev. Cancer* **2005**, *5* (7), 526–42.

(15) Haltiwanger, R. S.; Lowe, J. B. Role of glycosylation in development. *Annu. Rev. Biochem.* **2004**, *73*, 491–537.
(16) Moriwaki, K.; Okudo, K.; Haraguchi, N.; Takeishi, S.; Sawaki, H.; Narimatsu, H.; Tanemura, M.; Ishii, H.; Mori, M.; Miyoshi, E. Combination use of anti-CD133 antibody and SSA lectin can effectively enrich cells with high tumorigenicity. *Cancer Sci.* **2011**, *102* (6), 1164–70.
(17) Varki, A. Sialic acids in human health and disease. *Trends Mol. Med.* **2008**, *14* (8), 351–60.
(18) Yogeeswaran, G.; Salk, P. L. Metastatic potential is positively correlated with cell surface sialylation of cultured murine tumor cell lines. *Science* **1981**, *212* (4502), 1514–6.
(19) Fogel, M.; Altevogt, P.; Schirrmacher, V. Metastatic potential severely altered by changes in tumor cell adhesiveness and cell-surface sialylation. *J. Exp. Med.* **1983**, *157* (1), 371–6.
(20) Passaniti, A.; Hart, G. W. Cell surface sialylation and tumor metastasis. Metastatic potential of B16 melanoma variants correlates with their relative numbers of specific penultimate oligosaccharide structures. *J. Biol. Chem.* **1988**, *263* (16), 7591–603.
(21) Cui, H.; Lin, Y.; Yue, L.; Zhao, X.; Liu, J. Differential expression of the alpha2,3-sialic acid residues in breast cancer is associated with metastatic potential. *Oncol. Rep.* **2011**, *25* (5), 1365–71.
(22) Babal, P.; Janega, P.; Cerna, A.; Kholova, I.; Brabencova, E. Neoplastic transformation of the thyroid gland is accompanied by changes in cellular sialylation. *Acta Histochem.* **2006**, *108* (2), 133–40.
(23) Sethi, M. K.; Thaysen-Andersen, M.; Smith, J. T.; Baker, M. S.; Packer, N. H.; Hancock, W. S.; Fanayan, S. Comparative N-glycan profiling of colorectal cancer cell lines reveals unique bisecting GlcNAc and alpha-2,3-linked sialic acid determinants are associated with membrane proteins of the more metastatic/aggressive cell lines. *J. Proteome Res.* **2014**, *13* (1), 277–88.
(24) Lanctot, P. M.; Gage, F. H.; Varki, A. P. The glycans of stem cells. *Curr. Opin. Chem. Biol.* **2007**, *11* (4), 373–80.
(25) Taniguchi, N.; Ekuni, A.; Ko, J. H.; Miyoshi, E.; Ikeda, Y.; Ihara, Y.; Nishikawa, A.; Honke, K.; Takahashi, M. A glycomic approach to the identification and characterization of glycoprotein function in cells transfected with glycosyltransferase genes. *Proteomics* **2001**, *1* (2), 239–47.
(26) Hermann, P. C.; Huber, S. L.; Herrler, T.; Aicher, A.; Ellwart, J. W.; Guba, M.; Bruns, C. J.; Heeschen, C. Distinct populations of cancer stem cells determine tumor growth and metastatic activity in human pancreatic cancer. *Cell Stem Cell* **2007**, *1* (3), 313–23.
(27) Ross, P. L.; Huang, Y. N.; Marchese, J. N.; Williamson, B.; Parker, K.; Hattan, S.; Khainovski, N.; Pillai, S.; Dey, S.; Daniels, S.; Purkayastha, S.; Juhasz, P.; Martin, S.; Bartlet-Jones, M.; He, F.; Jacobson, A.; Pappin, D. J. Multiplexed protein quantitation in Saccharomyces cerevisiae using amine-reactive isobaric tagging reagents. *Mol. Cell Proteomics* **2004**, *3* (12), 1154–69.
(28) Zieske, L. R. A perspective on the use of iTRAQ reagent technology for protein complex and profiling studies. *J. Exp. Bot* **2006**, *57* (7), 1501–8.
(29) Kuno, A.; Uchiyama, N.; Koseki-Kuno, S.; Ebe, Y.; Takashima, S.; Yamada, M.; Hirabayashi, J. Evanescent-field fluorescence-assisted lectin microarray: a new strategy for glycan profiling. *Nat. Methods* **2005**, *2* (11), 851–6.
(30) Serada, S.; Fujimoto, M.; Ogata, A.; Terabe, F.; Hirano, T.; Iijima, H.; Shinzaki, S.; Nishikawa, T.; Ohkawara, T.; Iwahori, K.; Ohguro, N.; Kishimoto, T.; Naka, T. iTRAQ-based proteomic identification of leucine-rich alpha-2 glycoprotein as a novel inflammatory biomarker in autoimmune diseases. *Ann. Rheum. Dis.* **2010**, *69* (4), 770–4.
(31) Serada, S.; Fujimoto, M.; Takahashi, T.; He, P.; Hayashi, A.; Tanaka, T.; Hagihara, K.; Yamadori, T.; Mochizuki, M.; Norioka, N.; Norioka, S.; Kawase, I.; Naka, T. Proteomic analysis of autoantigens associated with systemic lupus erythematosus: Anti-aldolase A antibody as a potential marker of lupus nephritis. *Proteomics Clin. Appl.* **2007**, *1* (2), 185–91.
(32) He, P.; Naka, T.; Serada, S.; Fujimoto, M.; Tanaka, T.; Hashimoto, S.; Shima, Y.; Yamadori, T.; Suzuki, H.; Hirashima, T.; Matsui, K.; Shiono, H.; Okumura, M.; Nishida, T.; Tachibana, I.; Norioka, N.; Norioka, S.; Kawase, I. Proteomics-based identification of alpha-enolase as a tumor antigen in non-small lung cancer. *Cancer Sci.* **2007**, *98* (8), 1234–40.
(33) Shevchenko, A.; Wilm, M.; Vorm, O.; Mann, M. Mass spectrometric sequencing of proteins silver-stained polyacrylamide gels. *Anal. Chem.* **1996**, *68* (5), 850–8.
(34) Kuwamoto, K.; Takeda, Y.; Shirai, A.; Nakagawa, T.; Takeishi, S.; Ihara, S.; Miyamoto, Y.; Shinzaki, S.; Ko, J. H.; Miyoshi, E. Identification of various types of alpha2-HS glycoprotein in sera of patients with pancreatic cancer: Possible implication in resistance to protease treatment. *Mol. Med. Rep* **2010**, *3* (4), 651–6.
(35) Stojadinovic, A.; Hooke, J. A.; Shriver, C. D.; Nissan, A.; Kovatich, A. J.; Kao, T. C.; Ponniah, S.; Peoples, G. E.; Moroni, M. HYOU1/Orp150 expression in breast cancer. *Med. Sci. Monit* **2007**, *13* (11), BR231–239.
(36) Fukuda, M.; Viitala, J.; Matteson, J.; Carlsson, S. R. Cloning of cDNAs encoding human lysosomal membrane glycoproteins, h-lamp-1 and h-lamp-2. Comparison of their deduced amino acid sequences. *J. Biol. Chem.* **1988**, *263* (35), 18920–8.
(37) Privitera, S.; Prody, C. A.; Callahan, J. W.; Hinek, A. The 67-kDa enzymatically inactive alternatively spliced variant of beta-galactosidase is identical to the elastin/laminin-binding protein. *J. Biol. Chem.* **1998**, *273* (11), 6319–26.
(38) Eom, Y. W.; Kim, M. A.; Park, S. S.; Goo, M. J.; Kwon, H. J.; Sohn, S.; Kim, W. H.; Yoon, G.; Choi, K. S. Two distinct modes of cell death induced by doxorubicin: apoptosis and cell death through mitotic catastrophe accompanied by senescence-like phenotype. *Oncogene* **2005**, *24* (30), 4765–77.
(39) Hayase, T.; Rice, K. G.; Dziegielewska, K. M.; Kuhlenschmidt, M.; Reilly, T.; Lee, Y. C. Comparison of N-glycosides of fetuins from different species and human alpha 2-HS-glycoprotein. *Biochemistry* **1992**, *31* (20), 4915–21.
(40) Edge, A. S.; Spiro, R. G. Presence of an O-glycosidically linked hexasaccharide in fetuin. *J. Biol. Chem.* **1987**, *262* (33), 16135–41.
(41) Stefan, N.; Haring, H. U. The role of hepatokines in metabolism. *Nat. Rev. Endocrinol.* **2013**, *9* (3), 144–52.
(42) Wang, H.; Sama, A. E. Anti-inflammatory role of fetuin-A in injury and infection. *Curr. Mol. Med.* **2012**, *12* (5), 625–33.
(43) Inohara, H.; Raz, A. Identification of human melanoma cellular and secreted ligands for galectin-3. *Biochem. Biophys. Res. Commun.* **1994**, *201* (3), 1366–75.
(44) von Mach, T.; Carlsson, M. C.; Straube, T.; Nilsson, U.; Leffler, H.; Jacob, R. Ligand binding and complex formation of galectin-3 is modulated by pH variations. *Biochem. J.* **2014**, *457* (1), 107–15.
(45) Akar, U.; Chaves-Reyez, A.; Barria, M.; Tari, A.; Sanguino, A.; Kondo, Y.; Kondo, S.; Arun, B.; Lopez-Berestein, G.; Ozpolat, B. Silencing of Bcl-2 expression by small interfering RNA induces autophagic cell death in MCF-7 breast cancer cells. *Autophagy* **2008**, *4* (5), 669–79.
(46) Ohnishi, T.; Nakamura, O.; Ozawa, M.; Arakaki, N.; Muramatsu, T.; Daikuhara, Y. Molecular cloning and sequence analysis of cDNA for a 59 kD bone sialoprotein of the rat: demonstration that it is a counterpart of human alpha 2-HS glycoprotein and bovine fetuin. *J. Bone Miner. Res.* **1993**, *8* (3), 367–77.
(47) Martin, M. J.; Muotri, A.; Gage, F.; Varki, A. Human embryonic stem cells express an immunogenic nonhuman sialic acid. *Nat. Med.* **2005**, *11* (2), 228–32.

dx.doi.org/10.1021/pr5004399 | *J. Proteome Res.* XXXX, XXX, XXX–XXX

DIABETOLOGY & METABOLIC SYNDROME

RESEARCH Open Access

Low serum galectin-3 concentrations are associated with insulin resistance in patients with type 2 diabetes mellitus

Tsuyoshi Ohkura[1*], Youhei Fujioka[1], Risa Nakanishi[1], Hideki Shiochi[1], Keisuke Sumi[1], Naoya Yamamoto[1], Kazuhiko Matsuzawa[2], Shoichiro Izawa[1], Hiroko Ohkura[2], Etsuko Ueta[3], Masahiko Kato[1], Eiji Miyoshi[4], Shin-ichi Taniguchi[2] and Kazuhiro Yamamoto[1]

Abstract

Background: Galectin-3 is a family of soluble beta-galactoside-binding lectins that play many important regulatory roles in inflammation. Galectin-3-deficient mice have been shown to exhibit excess adiposity, hyperglycemia, insulin resistance and systemic inflammation. We investigated the association between serum galectin-3 and insulin resistance in patients with type 2 diabetes using a glucose clamp method.

Methods: This was a cross-sectional study. Twenty patients (mean fasting plasma glucose 7.6 mmol/L, HbA1c 7.2%, BMI 28.1 kg/m^2) underwent a meal tolerance test and glucose clamp test. Participants were given a test meal and plasma glucose and insulin were measured at 0, 30, 60, 120 and 180 min. The glucose disposal rate was measured during hyperinsulinemic-euglycemic glucose clamps. Serum galectin-3 levels were measured using the enzyme-linked immunosorbent assay method.

Results: The mean serum galectin-3 level was 5103 pg/ml. Galectin-3 levels correlated significantly with the glucose disposal rate ($R = 0.71$, $P < 0.001$), fasting insulin ($R = -0.56$, $P < 0.01$), homeostasis model assessment for insulin resistance ($R = -0.52$, $P < 0.05$), and the insulin sensitivity index ($R = 0.62$, $P < 0.005$). Galectin-3 levels also positively correlated with the serum adiponectin level ($R = 0.61$, $P < 0.05$), but not with the high-sensitive C-reactive protein and interleukin-6 and −10.

Conclusions: These results suggest that low levels of serum galectin-3 are associated with insulin resistance in patients with type 2 diabetes.

Keywords: Galectin-3, Insulin resistance, Type 2 diabetes mellitus

Background

Galectin-3 is a family of soluble beta-galactoside-binding lectins that play important regulatory roles in inflammation [1]. Galectin-3 has been reported to be a predictor of prognosis of heart failure [2]. In type 2 diabetes, it was reported that systemic galectin-3 is elevated in obesity and is negatively correlated with glycated hemoglobin [3]. Galectin-3 was also increased in the serum of patients with elevated C-reactive protein. Compared with hepatic and systemic venous serum, galectin-3 was higher in the portal venous serum suggesting that the splanchnic region is a major site of galectin-3 synthesis. The lower levels of galectin-3 in the hepatic venous serum compared with the portal venous serum demonstrate that galectin-3 is removed by the hepatic system.

However, the pathophysiology of galectin-3 in diabetes is not well-known. One report, using an animal model, found that galectin-3+/+mice developed delayed and sustained hyperglycemia in streptozotocin-induced diabetes, mononuclear cellular infiltration and reduced insulin content of islets [4]. This was also accompanied by the expression of proinflammatory cytokines [4]. Galectin-3−/−

* Correspondence: ohkura@med.tottori-u.ac.jp
[1]Division of Cardiovascular Medicine, Endocrinology and Metabolism, Department of Molecular Medicine and Therapeutics, Tottori University Faculty of Medicine, Yonago, Tottori, Japan
Full list of author information is available at the end of the article

mice were relatively resistant to diabetogenesis as evaluated by measurements of glycemia, quantitative histology and insulin. Thus, galectin-3 is involved in immune mediated beta cell damage and is required for diabetogenesis in this model of the disease. Another study has revealed that the role of endogenous galectin-3 in beta cell apoptosis in the inflammatory milieu that occurs during diabetes pathogenesis, implicates impairment of the mitochondrial apoptotic pathway as a key event in the protection from beta cell apoptosis in the absence of galectin-3 [5]. However, galectin-3 over-expression protected beta-cells from the cytotoxic effect of IL-1beta [6]. Moreover, Pang et al. showed that young (12-week-old) galectin-3 deficient mice fed a standard diet exhibited altered glucose homeostasis in the absence of obesity and associated abnormalities, thus suggesting a direct positive modulation of beta-cell function by galectin-3 independent of obesity-related inflammation [7]. A recent animal study reported that obese galectin-3−/− mice have increased body weight, total visceral adipose tissue, fasting blood glucose and insulin levels, homeostasis model assessment of insulin resistance (HOMA-IR), and markers of systemic inflammation compared with diet-matched wild-type animals [8]. Obesity induced by accelerated high fat diet in galectin-3-deficient mice was associated with systemic inflammation. Increased levels of interleukin (IL)-6 and reduced levels of IL-10 in the sera of obese galectin-3-deficient mice might contribute to amplified obesity-induced inflammation.

These results suggest that a low serum galectin-3 level is associated with hyperinsulinemia, insulin resistance and inflammation in type 2 diabetes. Furthermore, these reports suggest that a serum galectin-3 level is associated with beta cell function. Therefore, we hypothesize that low serum galectin-3 could be associated with insulin resistance and beta cell function in patients with type 2 diabetes. We measured serum galectin-3 levels in type 2 diabetes patients, and performed a glucose clamp method and a meal tolerance test (MTT) to evaluate insulin resistance and beta cell function.

Methods

Subjects

Twenty participants were subjected to a glucose clamp test and an MTT. Type 2 diabetes mellitus was diagnosed based on the criteria of the Japan Diabetes Society (JDS) [9]. The mean age of the patients was 53.6 years, mean BMI was 28.0 kg/m^2, mean waist circumference was 95.8 cm, mean fasting plasma glucose (FPG) was 7.60 mmol/L and mean HbA1c was 7.25% (55 mmol/mol) (Table 1). Patients with ischemic heart disease, heart failure, pancreatic disease, liver disease, renal failure, or those taking diabetogenic medications such as corticosteroids were excluded from the study. Seven patients were on diet therapy alone and 13 were using oral hypoglycemic agents, including five on α-glucosidase inhibitors, five on dipeptidyl peptidase inhibitors, three on sulfonylurea, three on glinides and three on biguanides. None of the patients were using thiazolidinediones or insulin injections.

This study was approved by the Ethics Committee of the Faculty of Medicine, Tottori University and was conducted in compliance with the ethical principles of the Declaration of Helsinki. Informed consent was obtained from all of the patients using a procedure approved by the Ethics Committee.

Table 1 Patient characteristics

N	20	Fasting insulin (pmol/L)	68.3 ± 41.6
Gender (male/female)	13/7	HOMA-IR	3.77 ± 2.33
Age (years)	53.6 ± 11.4	ISI	4.32 ± 2.26
BMI (kg/m^2)	28.0 ± 3.8	Insulinogenic index	97.3 ± 117.1
Waist circumstance (cm)	95.8 ± 8.8	AUC glucose (mmol/L•h)	19.6 ± 3.5
FPG (mmol/L)	7.60 ± 1.18	AUC insulin (pmol/L•h)	448.0 ± 265.4
HbA1c (NGSP) (%)	7.25 ± 0.71	AUC insulin/AUC glucose	23.8 ± 14.3
(mmol/mol)	(55 ± 8)	hs-CRP (mg/dL)	0.16 ± 0.13
LDL-C (mmol/L)	3.33 ± 0.85	IL-6 (pg/ml)	2.96 ± 3.52
TG (mmol/L)	1.80 ± 0.89	IL-10 (pg/ml)	4.15 ± 2.93
HDL-C (mmol/L)	1.29 ± 0.37	adiponectin (μg/mL)	6.76 ± 3.57
GDR (mg · kg^{-1} · min^{-1})	5.33 ± 2.04	Proinsulin (pmol/L)	3.73 ± 3.32
Galectin-3 (pg/mL)	5103 ± 2239	Proinsulin/insulin ratio	0.09 ± 0.10

Data are means ± standard deviation.
BMI, body mass index; HbA1c, hemoglobin A1c; *NGSP*, National Glycohemoglobin Standardization Program; *FPG*, fasting plasma glucose; *LDL-C*, low-density lipoprotein cholesterol; *TG*, triglyceride; *HDL-C*, high-density lipoprotein cholesterol; *HOMA-IR*, homeostasis model assessment of insulin resistance; *ISI*, insulin sensitivity index; *AUC*, area under the concentration–time curve; *hs-CRP* high-sensitive C reactive protein; *IL*, interleukin; *GDR*, glucose disposal rate.

Meal tolerance test

After fasting for at least 12 h, the participants visited a morning clinic and consumed a test meal (total calories 460 kcal, carbohydrates 56.5 g, fat 18.0 g; protein 18.0 g) prepared by the JDS (JANEF E460F18, Kewpie Corporation, Tokyo, Japan) [10]. Plasma glucose and insulin were measured at 0 (fasting), 30, 60, 120, and 180 min after the meal. Plasma glucose was measured using the glucose oxidase method and plasma insulin using chemiluminescent immunoassays (CLIA) (human insulin CLIA kits, Kyowa Medix, Tokyo, Japan). Plasma insulin was defined as immunoreactive insulin (IRI). This method, using the meal tolerance test (MTT), is a well-established method in our hospital [11,12].

HbA1c (JDS) was measured by high-performance liquid chromatography and was converted to National Glycohemoglobin Standardization Program (NGSP) values using the following certified equation, NGSP (%) = 1.02 × JDS (%) + 0.25% [13]. HbA1c (NGSP) values were also converted to International Federation of Clinical Chemistry (IFCC) values (mmol/mol) using the HbA1c converter developed by the National Institutes of Diabetes and Digestive and Kidney Diseases [14].

Euglycemic–hyperinsulinemic clamp

Glucose clamp studies were performed 2 days after the MTT. The patients were examined in the morning after an overnight fast. An antecubital vein was cannulated to administer the infusate. A dorsal vein was cannulated and kept warm to facilitate venous sampling and provide arterialized venous blood. Using an artificial endocrine pancreas (STG 55; Nikkiso, Shizuoka, Japan), the euglycemic–hyperinsulinemic clamp was performed to determine insulin sensitivity in peripheral tissues [15]. A primed constant infusion of insulin (100 $mU/m^2 \cdot min$) and computer-controlled exogenous infusion of glucose solution were used to achieve steady-state plasma insulin levels and maintain plasma glucose levels at 5.2 mmol/L (95 mg/dL). Using the insulin infusion protocol as previously reported, the steady-state plasma insulin level was 1200 pmol/L in patients with type 2 diabetes [16,17]. The steady-state glucose infusion rate (GIR) was calculated at 90–120 min, and the mean GIR during that time was used as a marker of peripheral insulin sensitivity. The mean GIR was defined as the glucose disposal rate (GDR). The glucose clamp method is a well-established procedure in our hospital [18]. Some of the data of the current study were already published in the previous study [18].

Galectin-3, adiponectin, hs-CRP, IL-6, IL-10 and proinsulin assays

An enzyme-linked immunosorbent assay (ELISA) kit was used for measuring galectin-3 (Human Galectin-3 Assay Kit, Immuno-Biological Laboratories Co., Gunma, Japan) [19], plasma adiponectin (human adiponectin ELISA kit, Otsuka, Tokyo, Japan), plasma high-sensitive C reactive protein (hs-CRP) (human hs-CRP ELISA kit, Otsuka, Tokyo, Japan), plasma interleukin-6 (IL-6) and interleukin-10 (IL-10) (human IL-6, IL-10 Quantikine ELISA, R & D Systems, Inc., Minneapolis, USA) and plasma proinsulin (human intact proinsulin ELISA kit, Biovendor, Heidelberg, Germany).

Calculation of insulin resistance and secretion indices

HOMA-IR was calculated by FPG (mmol/L) × fasting IRI (F-IRI pmol/L)/135 [20]. The insulin sensitivity index (ISI) was calculated by $10{,}000/\sqrt{\{[FPG\ (mmol/L) \times F\text{-}IRI\ (pmol/L)] \times [mean\ glucose \times mean\ insulin\ during\ MTT]\}}$ [21]. Insulinogenic index was measured by [insulin (pmol/L) at 30 min − insulin (pmol/L) at 0 min]/[glucose (mmol/L) at 30 min − glucose (mmol/L) at 0 min] [22].

Statistical analyses

Data are expressed as means ± standard error of the mean. The area under the curve (AUC) was calculated according to the trapezoidal rule. Correlations between parametric clinical variables and the galectin-3 were determined by Pearson's correlation analysis. Multiple regression analysis was performed to examine an influencing factor of the serum galectin-3 level, the independent variables were: age, gender, BMI, waist circumference, FPG, HbA1c, fasting insulin, HOMA-IR, Insulinogenic Index, GDR, hs-CRP, IL-6, IL-10, proinsulin/insulin ratio, adiponectin, and triglyceride (TG). Values of $P < 0.05$ were considered significant. SPSS software version 15.0 (SPSS, Chicago, IL, USA) was used for all analyses.

Results

Serum galectin-3 level of all participants was 5103 pg/mL (Table 1). The hs-CRP was 0.16 mg/d and adiponectin was 6.76 μg/mL. The FPG result of the MTT was 7.6 mmol/L, and the 2 h postprandial glucose was 10.6 mmol/L (Figure 1-a). Fasting insulin was 68.3 pmol/L and the 2 h postprandial insulin was 299.6 pmol/L (Figure 1-b). HOMA-IR was 3.77, ISI was 4.32 and the insulinogenic index was 97.3 (Table 1). During the steady state of glucose clamps, GDR was 5.33 $mg \cdot kg^{-1} \cdot min^{-1}$ and the insulin level was 1159 ± 411 pmol/L. All results are given as means.

Galectin-3 level strongly correlated with the GDR in the glucose clamp method ($R = 0.71$, $P < 0.001$) (Table 2, Figure 2-a). Galectin-3 level negatively correlated with fasting insulin ($R = -0.56$, $P < 0.01$) (Figure 2-b), and HOMA-IR ($R = -0.52$, $P < 0.05$) (Figure 2-c). Galectin-3 level also positively correlated with the ISI in MTT ($R = 0.62$, $P < 0.005$) (Figure 2-d) and with adiponectin ($R = 0.61$, $P < 0.05$) (Figure 2-e). The AUC of glucose did not correlate with galectin-3 ($R = -0.02$, $P = 0.92$).

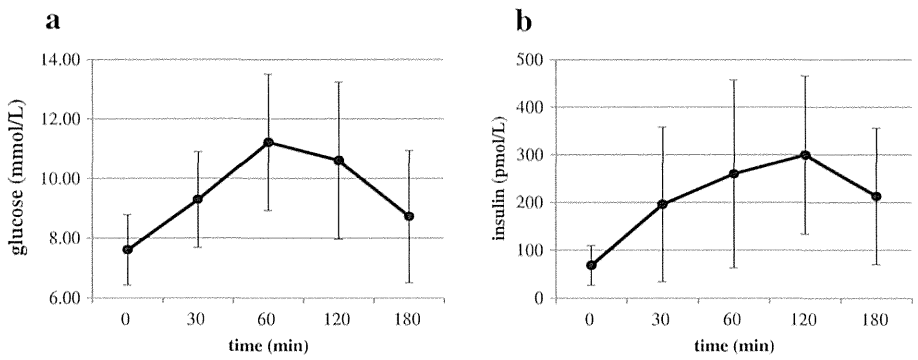

Figure 1 Plasma glucose and insulin responses during the meal tolerance test. Plasma glucose response during the meal tolerance test **(a)**, and insulin response **(b)** during the meal tolerance test.

The AUC of insulin and the ratio of AUC-insulin/AUC-glucose had a tendency to correlate with galectin-3, but this was not significant (R = −0.41, P = 0.06; R = −0.44, P = 0.05, respectively) (Table 2). The insulinogenic index had a tendency for negative correlation with galectin-3, but was not significant (R = −0.22, P = 0.33) (Table 2).

Table 2 Correlation coefficients between serum galectin-3 concentrations and other parameters

Correlation of galectin-3 with	Pearson correlation	P value
GDR	0.71	< 0.001
Fasting insulin	−0.56	< 0.01
HOMA-IR	−0.52	< 0.05
ISI	0.62	< 0.005
Insulinogenic Index	−0.22	0.33
AUC glucose	−0.02	0.92
AUC insulin	−0.41	0.06
AUC insulin/AUC glucose	−0.44	0.05
hs-CRP	−0.25	0.27
IL-6	0.08	0.75
IL-10	−0.15	0.53
Proinsulin/insulin ratio	0.30	0.20
adiponectin	0.61	< 0.05
BMI	−0.17	0.48
waist circumference	−0.24	0.29
FPG	0.11	0.61
HbA1c	−0.10	0.66
LDL-C	0.27	0.23
TG	−0.14	0.52
HDL-C	0.28	0.21

Correlation coefficients were determined using Pearson's product moment correlation coefficient test.
GDR, glucose disposal rate; *HOMA-IR*, homeostasis model assessment of insulin resistance; *ISI*, insulin sensitivity index; *AUC*, area under the concentration–time curve; *hs-CRP*, high-sensitive C reactive protein; *IL*, interleukin; *BMI*, body mass index; *FPG*, fasting plasma glucose; *LDL-C*, low-density lipoprotein cholesterol; *TG*, triglyceride; *HDL-C*, high-density lipoprotein cholesterol.

The proinsulin/insulin ratio had a tendency for positive correlation with galectin-3, but again, was not significant (R = 0.30, P = 0.20) (Table 2, Figure 2-f). There were no significant correlations between galectin-3 and FPG, HbA1c, BMI, waist circumstance, lipid profiles, hs-CPR, IL-6 and IL-10 (Table 2).

Using multiple regression analysis, we examined influence factors of serum galectin-3 level. The independent variables were: age, gender, BMI, waist circumference, FPG, HbA1c, fasting insulin, HOMA-IR, Insulinogenic Index, GDR, hs-CRP, IL-6, IL-10, proinsulin/insulin ratio, adiponectin, and TG. The significant standard partial regression coefficient was GDR 0.898 (P < 0.05) (Table 3).

Discussion

This study indicates that low serum galectin-3 concentrations strongly correlates with insulin resistance and hyperinsulinemia, evaluated by glucose clamp method, HOMA-IR, and ISI. Another study reported that obese galectin-3 knockout mice had increased fasting blood glucose and insulin levels, HOMA-IR and markers of systemic inflammation compared with diet-matched wild type animals [8]. Our study indicates that low levels of serum galectin-3 in patients with type 2 diabetes have insulin resistance and hyperinsulinemia similar to galectin-3 knockout mice. Although the area under the curve for glucose, for insulin and for the ratio insulin/glucose was not significantly associated with galectin-3 levels, there were significant associations between galection-3 and GDR, HOMA-IR, and ISI. These results suggested that the concentration of galectin-3 mainly affects insulin resistance rather than glucose levels.

Furthermore, galectin-3 was strongly correlated with adiponectin, which is an insulin sensitizer molecule. Pang et al. demonstrate the development of excess adiposity and systemic inflammation in galectin-3 deficiency that was associated with impaired fasting glucose levels and reduced adipose tissue expression of adiponectin and PPARγ [7]. These results suggest that the concentrations